Appendix A Chemical Compatibility Tests on CPVC and LEXAN

Two polymers, CPVC and LEXAN, were selected as candidates for portions of the flow loop. Solution leaching tests for the candidate polymers were performed to support the design of the flow loop. The leaching tests at were performed at 200°F in ultra high purity (UHP) water; in a solution with B 2800-ppm, Li 3-ppm, HCl 100-ppm, and pH = 10 with NaOH additions; and in a solution with B 2800-ppm, Li 3-ppm, HCl 100-ppm, and pH = 7 from trisodium phosphate additions.

A1. Weight change

The test samples were prepared from samples of CPVC and LEXAN tubing. The physical shape for both polymers was made identically for targeting the direct comparison on the compatibility. The test was performed in open air in quartz containers with a cooling condenser to avoid changes in the solution during the test. The test results are summarized in Fig. A1 and Table A1. Both the CPVC and LEXAN gained weight by water absorption.

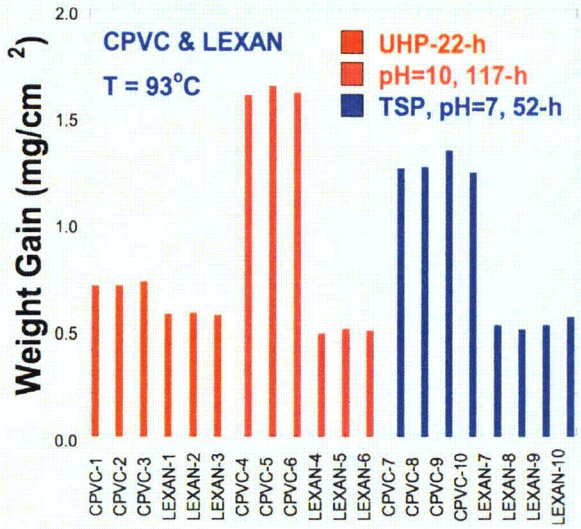

Figure A1.
Compiled weight change data for the CPVC and LEXAN exposed time period 22 to 117-h at 93 °C in the UHP-water, pH = 10.0 solution, and pH = 7.0 TSP solutions.

Transparent corrosion products were observed in both the CPVC and LEXAN tests. The products grew into large thin flat crystals (1.0-1.5 cm sharp leaf shape) during the tests. When agitated slightly with a glass bar, the large thin crystals disintegrated into fine fragments (1-mm size) and settled down to the bottom of the chambers. The container with CPVC samples had more corrosion product than the container with the LEXAN samples, and it showed qualitatively more corrosion product than that of LEXAN throughout the test. All the samples gained weight due to the absorption during the leaching test as shown in Figs. A1-A3. However, if the sample was dried in air for a weekend (70-h), most of the absorbed water in the LEXAN was released, but about 30% was left in the CPVC as shown in Fig. A2.

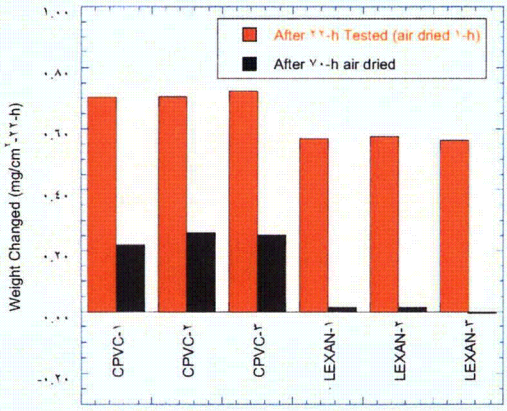

Figure A2
Weight change (mg/cm^2) vs. various samples for 22-h leaching test at T= 93˚C.

Table A1. Compiled weight change data for the CPVC and LEXAN exposed time period at 93 ˚C in the UHP-water, pH = 10.0 solution, and pH = 7.0 TSP solution.*

	#	Solution	Wi (g)	Wf (g)	ΔW (g)	A(cm^2)	ΔW/A (mg/cm^2)	Note
CPVC	1	UHP	1.073	1.078	0.005	6.96	0.70	Wt. gain by water absorption
	2	93˚C	1.046	1.051	0.005	6.81	0.70	
	3		1.168	1.174	0.005	7.49	0.72	
LEXAN	1	22-h	1.377	1.382	0.006	9.98	0.57	
	2		1.399	1.405	0.006	10.1	0.57	
	3		1.323	1.329	0.005	9.66	0.56	
CPVC	4	pH =	1.076	1.087	0.011	6.98	1.59	Wt. gain by water absorption
	5	10.0	1.152	1.164	0.012	7.40	1.64	
	6	93˚C	1.348	1.361	0.014	8.48	1.61	
LEXAN	4		1.393	1.398	0.004	10.08	0.48	
	5	116-h	1.469	1.474	0.005	10.54	0.500	
	6		1.430	1.435	0.005	10.31	0.49	
CPVC	7	pH =	1.043	1.052	0.008	6.73	1.25	Wt. gain by water absorption and loosed by the corrosion product transferred into the solutions
	8	7.0	1.109	1.118	0.009	7.16	1.26	
	9		0.964	0.972	0.008	6.22	1.34	
	١	TSP	0.919	0.927	0.007	5.93	1.23	
LEXAN	7	93˚C	0.682	0.684	0.002	3.94	0.52	
	8		0.931	0.934	0.003	5.38	0.49	
	9	52-h	0.906	0.908	0.003	5.23	0.52	
	١		0.910	0.913	0.003	5.26	0.56	

*Wi initial weight; Wf final weight; ΔW=Wf-Wi; A area of sample exposed

A2. Electrical conductivity and SEM/EDS analysis of leachants

In-situ electrical conductivity was also monitored throughout the leaching tests. The leached solutions were dried and the residues examined by SEM/EDS.

Ultra high purity (UHP) water

The in-situ electrical conductivity during the leaching tests is shown in Fig. A3. The electrical conductivity measured and determined by EIS analysis within the frequency ranges between 1-Hz and 300-kHz for leaching in UHP water near 93°C for the period between 6 and 22-h for as received CPVC and LEXAN.

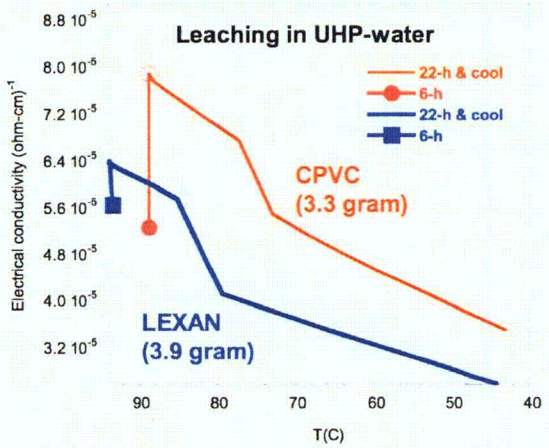

Figure A3.
The electrical conductivity measured and determined by electrochemical impedance spectroscopy (EIS) analysis within the frequency ranges between 1-Hz and 300-kHz for leaching in UHP water near 200˚F for periods of 6-h (closed symbols) and 22-h (open symbols) for CPVC (circle symbols) and LEXAN (square symbols).

The organic polymer residues left after the leached solution was dried were examined by SEM/EDS. The residue of the LEXAN leached solution dried on the platinum foil under vacuum had a long (2-3 mm long) fiber form as shown in Fig. A4(a), likewise the residue of the CPVC leached solution had a similar fiber form as shown in Fig. A4(b) and A4(c).

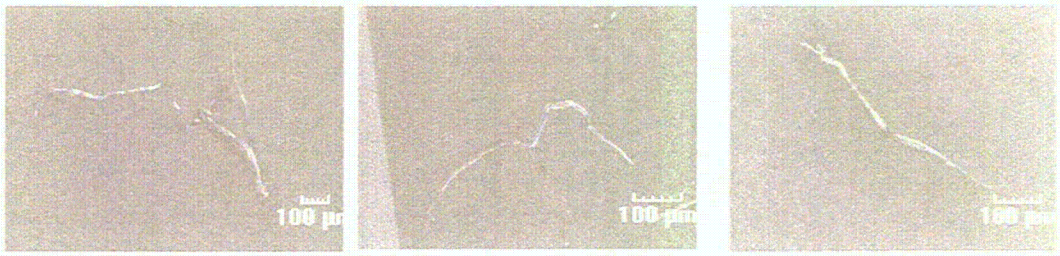

(a) (b) (c)
Figure A4. EDS view for the fiber form residue on the platinum for the (a) LEXAN; (b) and (c) CPVC leached solution.

NaOH buffer pH = 10

The conductivities of the solutions during the tests in the NaOH environment are shown in Fig. A5 as the ratio of conductivity at time t, $\sigma(t)$ to the initial conductivity, $\sigma(0)$. The CPVC has a higher leaching rate and a higher absorption rate than the LEXAN in both the UHP-water and the pH = 10.0 solution

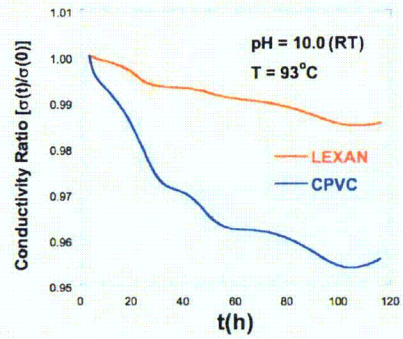

Figure A5.
Ratio of conductivity at time t with initial conductivity during the leaching test at 293°C in the pH = 10.0 solution for the LEXAN and the CPVC leaching test in the 125-ml solutions.

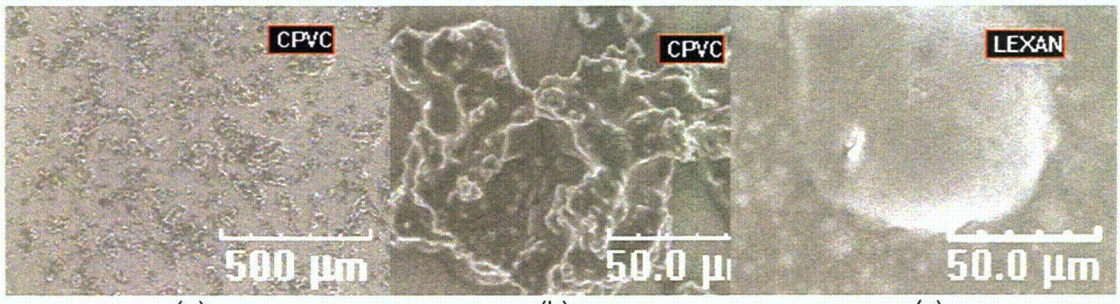

(a) (b) (c)

Figure A6. (a) SEM views for the dried from the CPVC leached pH = 10 solution, (b) extended view from (a), and (c). LEXAN leached pH = 10.0.

The conductivity results suggest that the leaching has greatly slowed after ≈ 100 h. The residues after drying are shown in Fig. A6.

pH = 7 (RT) TSP solution

The conductivity in the TSP solution is shown in Fig. A7 in terms of the ratio of conductivity at time t, $\sigma(t)$, with initial conductivity, $\sigma(0)$.

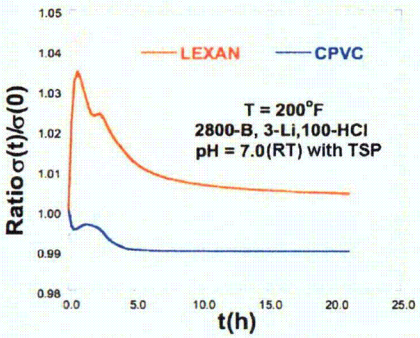

Figure A7.
Ratio of conductivity at time t with initial conductivity during the leaching test at 93°C in the pH = 7.0 (RT) solution for the LEXAN (3.5-g) and the CPVC (4-g) leaching test in the 125-ml solutions.

Based on the results our leaching tests, it can be concluded that the CPVC has higher leaching and also water absorption rate than the LEXAN in the UHP-water and in the pH = 10.0 solution, but CPVC less absorption in the pH = 7.0 TSP solution. No clouding of the LEXAN was observed nor was cracking observed in either of the materials in any of the environments.

Appendix B Cal–Sil leaching tests

B1. Background

The Cal–Sil leaching tests for the ICET-3 environments focused on temperatures between 60 and 85°C, a pH range between 4 and 10, and times between 5 min and 15 days.

Preliminary experiments were performed to compare the dissolution rate of pulverized Cal–Sil and a much coarser Cal–Sil debris, roughly 6 x 6 x 6 mm blocks. The two types of debris were exposed to a simulated sump solution with 2800-ppm-B, 7-ppm-Li, and 100-ppm-HCl and TSP additions to adjust the solution pH to 7.0. Electrical conductivity was used to continuously monitor the Cal–Sil dissolution. Figure B1(a) shows the electrical conductivity of the solution vs. time of exposure for the two types of Cal–Sil/l debris, and for the solution without debris. Figure B1(b) shows the net variation of electrical conductivity vs. time after subtracting off the contribution from the solution. The dissolution kinetics of the two types of debris are quite similar. The very high porosity of the Cal–Sil makes the leaching kinetics of the nominally solid blocks comparable to the pulverized Cal–Sil. A SEM picture of the pulverized Cal–Sil is shown in Fig. B2.

The chemical composition of the Cal–Sil is shown in Table B1. The composition is consistent with the assumption that Cal–Sil is primarily $CaSiO_3$. The dominant elements are Ca (21%) and Si (17%), but there are also about 2% alkali metals present. The Na and K compounds will dissolve rapidly and increase the pH. Ca also tends to increase the pH, but the Ca compounds will dissolve more slowly.

Dissolved Ca reacts quickly with anions such as PO_4^{-3}in aqueous environments. The solubility of most Ca-compounds is very low compare with the other inorganic compounds, and Ca-compounds typically have retrograde solubility, i.e., the solubility decreases with increasing temperature. The solubility of $Ca_3(PO_4)_2$ at pH = 6.8–7.1 in the presence of excess phosphate is shown in Fig. B3.

When trisodium phosphate is added to the leached Cal–Sil solution, the calcium and phosphate can combine to form a variety of compounds. X–ray diffraction studies at the University of New Mexico by K. Howe and D. Cheng (Fig. B4) show that the spectrum from deposits in the ICET–3 test match well with $Ca_3(PO_4)_2 \cdot x\ H_2O$ (tricalcium phosphate hydrate), $Ca_5(PO_4)_3(OH)$ (hydroxyapatite), and $Ca_9HPO_4(PO_4)5OH$ (calcium hydrogen phosphate hydroxide).

For simplicity the chemical reaction of the Ca and silicate leached from the Cal–Sil with the trisodium phosphate can be considered as

$$3Ca^{+2} + 3SiO_3^{-2} + 6Na^{+} + 2PO_4^{-3} = Ca_3(PO_4)_2\downarrow + 6Na^{+} + 3SiO_3^{-2} \qquad \text{(B1)}$$

with $Ca_3(PO_4)_2$ as the primary precipitation product. As discussed previously, at the temperatures of interest in the sump $Ca_3(PO_4)_2$ is relatively insoluble (Fig. B3).

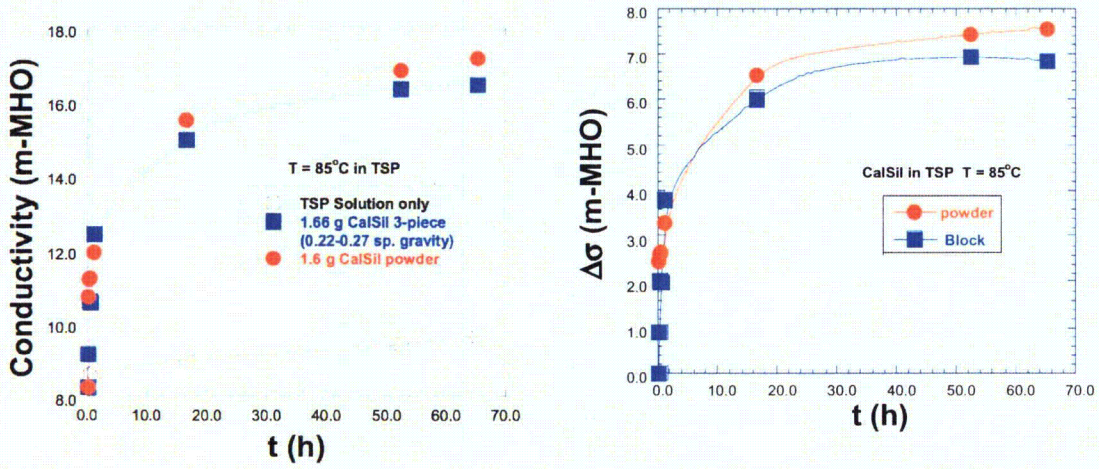

(a) (b)

Figure B1 (a) Measured electrical conductivity change of the solution during the leaching of Cal–Sil blocks and powder in an ICET-3 type solution at 85°C with B = 2800-ppm, Li = 3-ppm, HCl = 100-ppm in pH = 7.0 by TSP addition, and (b) the net variation of electrical conductivity vs. t after subtracting the contribution of the base TSP solution,

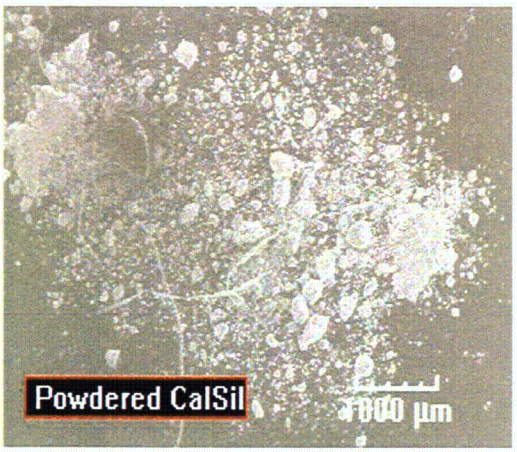

Figure B2
Powdered Cal–Sil.

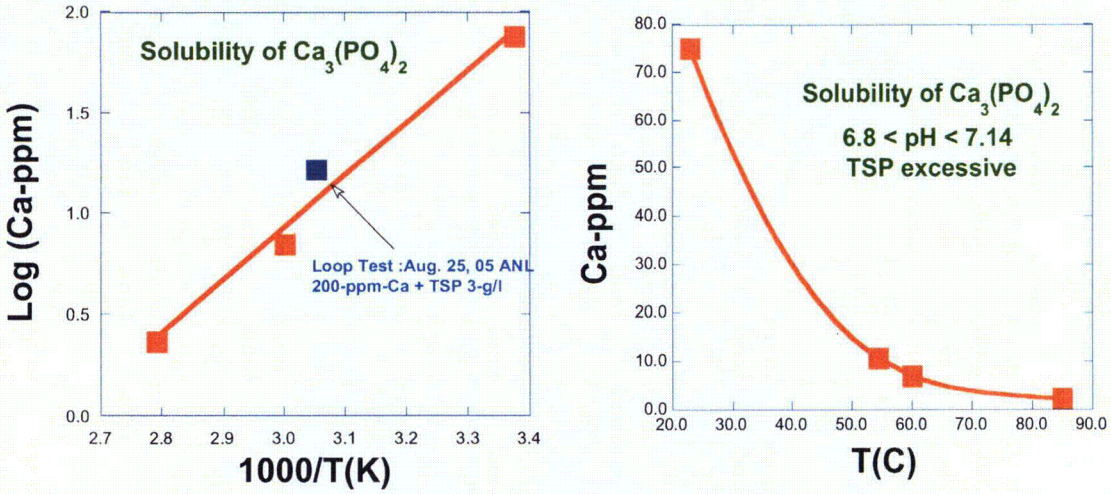

Figure B3. Log Ca (ppm) in the saturated solution of $Ca_3(PO_4)_2$ vs. inverse temperature(K) and T(C).

Table B1. Elemental ICP-analysis for the as–received Cal–Sil

			06-0015-01		06-0015-01 Dup		06-0015-02		06-0015-03				
	Oxide	Oxide Factor	Element, %	Oxide, %	Element, %	Oxide, %	Element %	Oxide, %	Element %	Oxide %	Moles	Anions, eq	Cations, eq
Al	Al_2O_3	0.52925	3.25	6.14	3.07	5.80	3.17	5.99	2.99	5.65	0.1103		0.332
Ca	CaO	0.7147	21.4	29.94	20.2	28.26	21.2	29.66	20.4	28.54	0.5090		1.018
Fe	Fe_2O_3	0.69943	1.74	2.40	1.68	2.40	1.7	2.43	1.6	2.29	0.0285		0.086
Mg	MgO	0.603		0.00		0.00		0.00	0.4	0.66	0.0165		0.033
K	K_2O	0.8302	0.36	0.43	0.36	0.43	0.36	0.43	0.41	0.49	0.0105		0.010
Si	SiO_2	0.4674	17.0	36.36	17.1	36.59	17.6	37.66	16.1	35.09	0.5999	1.199	
Na	Na_2O	0.7419	1.33	1.79	1.24	1.67	1.47	1.98	2.59	3.49	0.1127		0.113
Ti	TiO_2	0.5995		0.00		0.00		0.00	0.14	0.23	0.0029		0.006
C	CO_2	0.273		0.00		0.00		0.00	3.03	11.10	0.2522	0.504	
S	SO_3	0.4		0.00		0.00		0.00	0.288	0.72	0.0090	0.018	
											Sum:	1.80	1.80
	Sum:			79.09		76.16		78.15		88.27			
			Material might not be uniform in composition					LOI 104C		4.170			
								LOI 1000C		16.691			
								LOI 1000C-CO2:		5.79	= "Bound Water"		
								Total Mass Recovery, %		98.23			
								Total loss on heating to 1000C, wt%			Sum:	21. 80	
Ca/S Mol Ratio				0.828		0.826		0.844		0.872			
Na/S Mol Ratio				0.091		0.089		0.102		0.109			

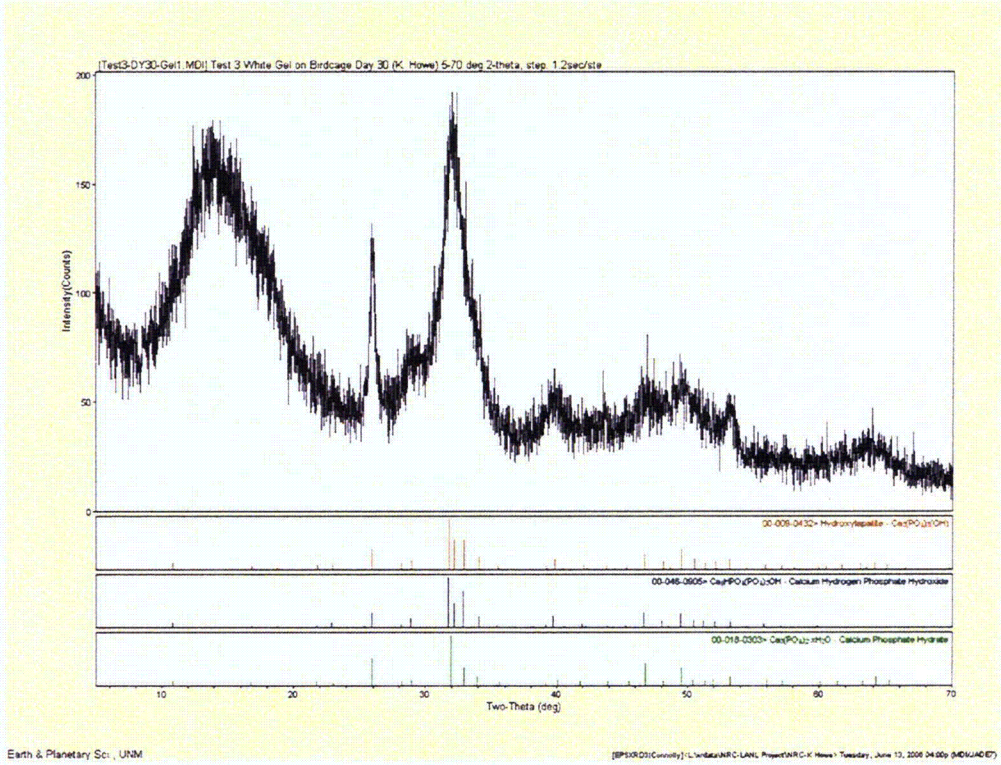

Figure B4. X–ray diffraction spectrum of deposits from the ICET–3 test and matches with $Ca_3(PO_4)_2 \cdot x\ H_2O$ (tricalcium phosphate hydrate), $Ca_5(PO_4)_3(OH)$ (hydroxylapatite), and $Ca_9HPO_4(PO_4)5OH$ (calcium hydrogen phosphate hydroxide)

B2. Initial Rate of Dissolution

Electrical conductivity and pH measurements were used to monitor the initial, relatively rapid dissolution of Cal–Sil when it is added to simulated sump solutions. The behavior of the conductivity and pH for the first 10 minutes after 1.2 g of Cal–Sil was added to 200 ml of base solution (6 g/l) with B = 2800-ppm, Li = 3-ppm, HCl = 100-ppm at 60°C are shown in Fig. B5. There is a rapid increase within a few minutes in both pH and conductivity. The rate of change and presumably the rate of dissolution slows significantly after 4 to 5- min have passed.

A second test was performed with a higher loading 25 g/l of Cal–Sil for 120 min. Again the conductivity and pH rise very rapidly initially. With the higher loading of Cal–Sil the initial pH $\approx$ 4 increases to $\approx$ 6.8. The decrease in dissolution rate is due in part to the increase in pH from the dissolution of the Na_2SiO_3 present in Cal–Sil. More importantly, for these high loadings, the dissolved Ca probably reaches a saturation value which inhibits further dissolution of the $CaSiO_3$. If TSP were present, the phosphate would combine with the Ca and remove it from solution and permit the dissolution of the Cal–Sil to continue.

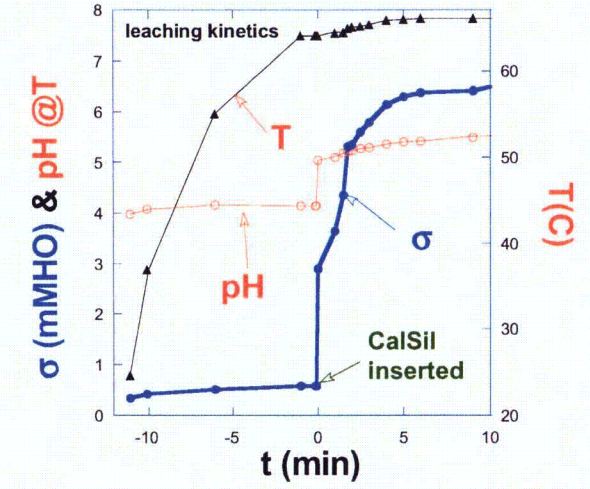

Figure B5.
Leaching kinetics for the initial 10-min after addition of 6 g/l Cal–Sil at t = 0.

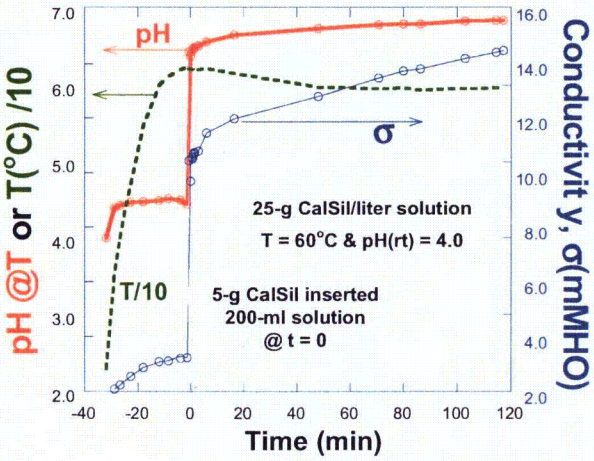

Figure B6.
Leaching kinetics for the initial 120-min after addition of 25 g/l Cal–Sil at t = 0. The temperature is plotted as T/10 for convenience.

A series of tests were performed with Cal–Sil loadings ranging from 2.0 to 166.0-g/l, and different initial pH values achieved by additions of HCL or NaOH. The results of the tests are shown in Table B2. Although the initial pH is controlled, for the solutions that are initially acidic, the final pH tends to increase as material is leached from the Cal–Sil. Except for the shortest exposure of 35 minutes, the Ca level in the solution is essentially independent of the Cal–Sil loading over the range from 6-166 g/l, although it is markedly smaller for the case of 2 g/l.

More detail on the sequence of tests with initial pH = 4.51 is given in Table B3 and Fig. B7. The Na levels increase with loading as expected for a species that is not approaching a solubility limit. The pH increases with increasing Cal–Sil loading consistent with the rise in the Na level. The Ca concentration is almost independent of loading except perhaps at the highest loading where it decreases. This may be due to a change in solubility at the relatively high pH associated with the high Cal–Sil loading.

Table B2. Compiled data for the Cal–Sil leaching performed in the various pH and temperatures.

No.	Leaching					Ca (ppm)	Note
	Solution, pH (RT)	T(C)	time	Cal–Sil-g/l	Final Solution pH (RT)		
1	4.00	60	35 min	6	7.52	176	Solution pH = 4.0 $B(OH)_3$ + Li(OH) + HCl
2	4.00	60	35 min	15	6.87	256	
3	4.00	60	35-min	25	6.78, 6.66@T	244	
4	4.00	60	35-min	166	6.50	228	
5	4.00	60	4-h	6	6.74/*6.74	196	
6	4.00	60	4-h	15	6.91/*6.94	195	
7	4.00	60	4-h	25	7.09/*7.05	195	
8	4.00	60	4-h	166	7.71/*7.68	168	
9	4.51	60	4-h	6	6.72	156	Solution pH = 4.5 $B(OH)_3$ + Li(OH) + HCl
10	4.51	60	4-h	15	6.87	169	
11	4.51	60	4-h	25	7.12	184	
12	4.51	60	4-h	166	7.98	127	
13	6.80	85	2-h	166	-	22	UHP: Pure water
14	7.00	85	2-h	-	-	2	No 13 (pure water) supernate solution +TSP
15	7.00	60	2-h	$CaCl_2$	6.80	7	Ca-200-ppm by $CaCl_2$ reacted with TSP; Cal–Sil leaching at rt > 60°C.
16	7.00	rt	2-h	$CaCl_2$	-	75	
17	7.00	54.3	~2 h	0.13	7.00	11	Loop Test #1, pH = 7.0 by TSP excess
18	7.00	62	4-h	2	7.14	45	Solution pH =7 made by $B(OH)_3$ + Li(OH) + HCl + NaOH addition (No TSP added)
19	7.00	62	4-h	6	7.37	88	
20	7.00	62	4-h	25	7.24	69	
21	7.00	62	24-h	2	7.19	73	
22	7.00	62	24-h	6	7.27	108	
23	7.00	62	24-h	25	7.42	102	
24	10.06	60	3.5-h	6	10.04	17	Solution pH = 10.0 made by $B(OH)_3$ + Li(OH) + HCl + LiOH excess addition (No TSP added)
25	10.06	60	3.5-h	15	9.99	18	
26	10.06	60	3.5-h	25	9.94	19	
27	10.06	60	3.5-h	166	9.73	22	

Table B3. Elemental chemical analysis (in mg/l) by the ICP emission spectra for the Cal Sil leached solution of pH = 4.51 at 60°C for 4-hrs

Loading	166-g Cal–Sil/l		25-g Cal–Sil/l		15-g Cal–Sil/l		6-g Cal–Sil/l	
Element	start	end	start	end	start	end	start	end
Ca	none	127.0	none	184.0	none	169.0	none	156.0
Si	none	113.0	none	66.40	none	51.40	none	49.00
Na	none	1500.	none	386.0	none	237.0	none	169.0
pH	4.51	7.85	4.51	7.12	4.51	6.87	4.51	6.76

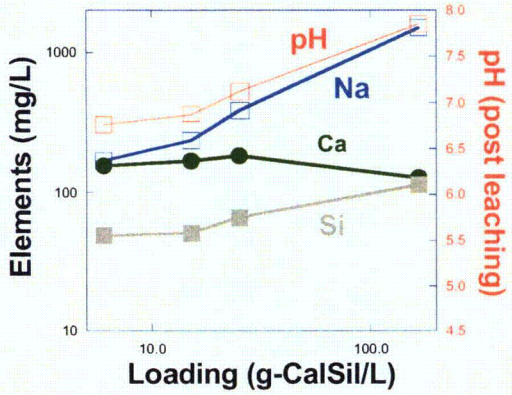

Figure B7.
Elemental chemical concentration determined by ICP analysis and final pH for solutions with different Cal–Sil loadings

B3. Benchmark tests with $CaSiO_3$

Leaching tests were performed with commercial $CaSiO_3$ to help benchmark results with Cal–Sil. The Cal–Sil loading was 25-g/l in a base solution with 2800-ppm-B and 0.7-ppm-Li at 60°C with the initial pH = 7.14 adjusted by adding either NaOH or TSP.

The test results for the dissolved Ca and Na for solutions in which the pH is controlled by NaOH additions are shown in Fig. B8 (a) for Cal–Sil and in B8 (b) for $CaSiO_3$. As expected in the Cal–Sil, the concentrations of the Na and Ca increase linearly with the dissolved Si level corresponding to the dissolution of Na_2SiO_3 and $CaSiO_3$. The slope of the Na curve is again as expected somewhat steeper than the Ca curve. For the case of $CaSiO_3$, the Na curve is flat since there is no Na_2SiO_3, but the Ca concentration does increase linearly with the Si concentration. However, the actual values of the Ca concentrations are shifted upwards about 50 ppm from those expected based on stoichiometric dissolution. This 50-ppm-Ca shift could be from a surface carbonate or hydroxide that formed on the chemicals due to exposure to the atmosphere or from the dissolution of other Ca compounds present in the Cal–Sil.

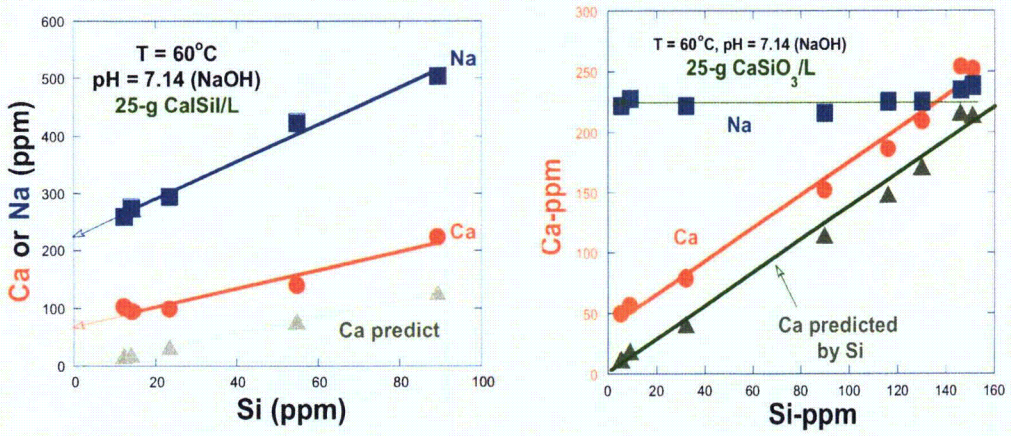

(a) (b)

Figure B8. Concentration of the elements in the solution with 25 g/l loading and pH = 7.14 with NaOH as a function of Si in solution (a), Cal–Sil and (b), $CaSiO_3$.

Dissolved Ca and Na levels for solutions in which the pH is controlled by TSP additions are shown in Fig. B9 for Cal–Sil and in Fig. B10 for $CaSiO_3$. In these tests there is excess Ca present and at about 100 h all the phosphate is consumed.

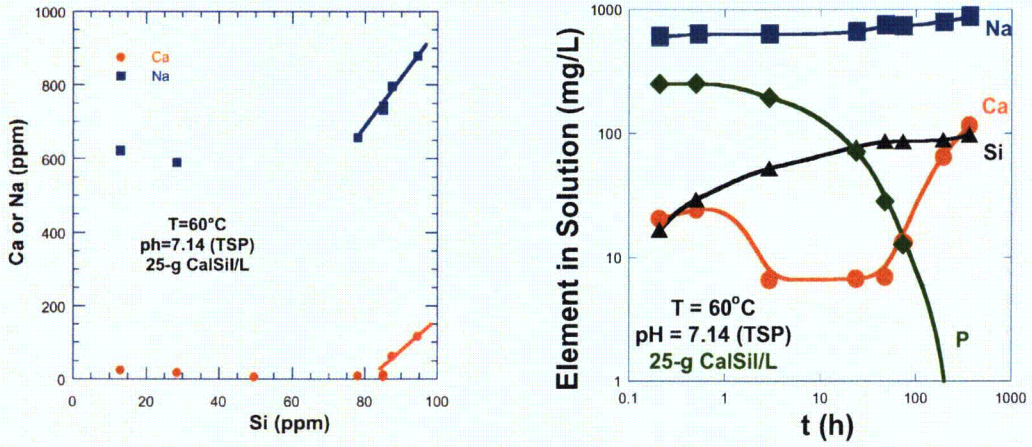

(a) (b)

Figure B9. Concentration of the elements in the solution as a function of leaching time (a) linear plot (b) log-log plot of (a) for the 25-g Cal–Sil/l loading pH = 7.14 with TSP.

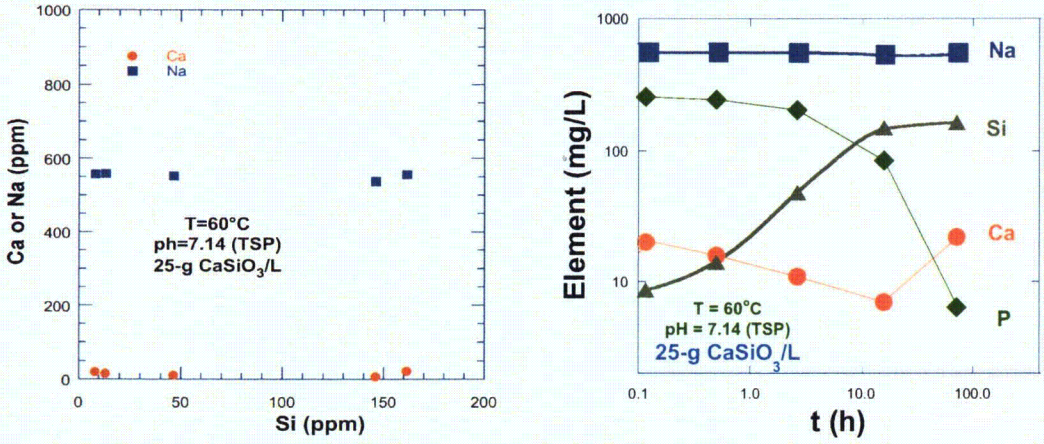

(a) (b)

Figure B10. Concentration of the elements in the solution as a function of leaching time (a) linear plot (b) log-log plot of (a) for the 25-g $CaSiO_3$/l loading pH = 7.14 with TSP

Table B4. *Compiled results on the leaching tests of the Cal–Sil insulator & commercial $CaSiO_3$ chemical vs. time: Loading 25-g/l, T = 60°C, and pH = 7.14 adjusted by adding NaOH or TSP*

Sample / Test condition		Leaching progress			Leaching Rate	
		t (h)	Ca (ppm) in solution	Ca (ppm) leached	Avg. t (h)	Leaching rate (Ca-ppm/h)
A	25-g Cal–Sil/l	0.12	103	103	0.06	858
	T = 60°C.	0.50	96	96	0.31	190
	pH = 7.14	2.67	99	99	2.59	2
	(NaOH)	16.00	140	140	9.34	3
		72.00	224	224	44.00	2
B	25-g Cal–Sil/l	0.12	106	106	0.60	833
	T = 60°C.	0.50	90	90	0.31	180
	pH = 7.14	2.67	110	110	2.59	9
	(NaOH)	16.00	152	152	9.34	3
		72.00	203	203	44.00	1
C	25-g $CaSiO_3$/l	0.12	20	36	0.05	360
	T = 60°C.	0.50	16	53	0.40	28
	pH = 7.14	2.67	11	128	1.60	34
	(TSP)	16.00	7	356	9.35	17
		72.00	22	522	44.00	297
D		0.26	50	50	0.13	191
	25-g $CaSiO_3$/l	0.51	56	56	0.38	337
	T = 60°C.	2.75	79	79	1.63	10
	pH = 7.14	23.83	152	152	12.79	5
	(NaOH)	47.64	186	186	35.74	2
		72.89	209	209	60.26	1
		192.50	252	252	132.70	0
		362.00	254	254	277.25	0
E		0.21	21	28	0.10	131
		0.50	25	26	0.25	51
	25-g Cal–Sil/l	2.92	7	136	1.71	46
	T = 60°C.	23.83	7	380	13.37	11
	pH = 7.14	47.61	7	465	35.72	4
	(TSP)	72.89	13	501	60.25	1
		192.50	65	577	132.70	0.64
		362.00	116	629	277.25	0.30

Amount of $Ca_3(PO_4)_2$ Sediment: Figure B11 shows the concentration of Ca and P in the sediment vs. time during leaching in pH = 7.14 (TSP), and (b) re-plot as log t for the 25-g Cal–Sil/l loading pH = 7.14 with TSP at 60°C. The assumption is the precipitate is $Ca_3(PO_4)_2$. This assumption is consistent with the studies at the University of New Mexico and measurements of the composition of the precipitate at ANL.

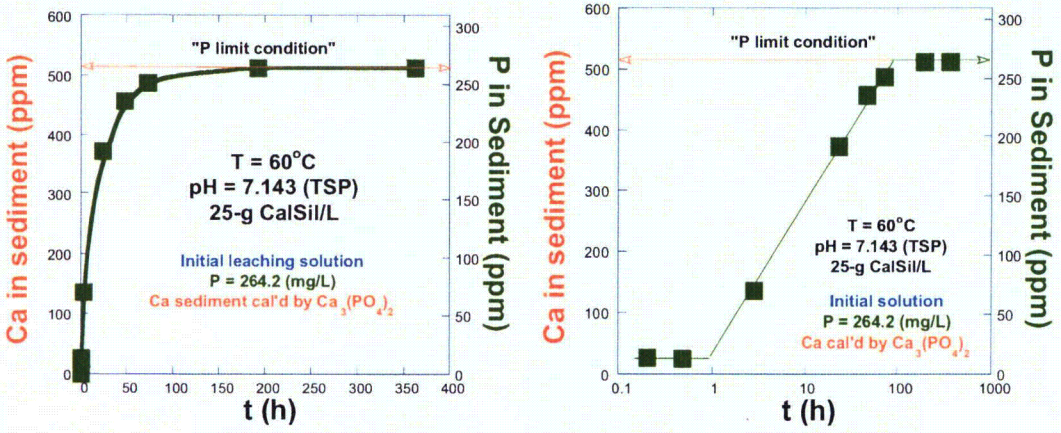

Figure B11. (a) Ca and P in the sediment vs. time during leaching in pH = 7.14 (TSP), and (b) re-plot as log t of (a) for the 25-g Cal–Sil/l loading pH = 7.14 with TSP.

B4. Influence of TSP dissolution rate

The dissolution of the Cal–Sil can be influenced by pH and the presence of phosphate to remove dissolved Ca as a precipitate. Thus the dissolution of the Cal–Sil could be affected by the rate at which TSP enters the sump. Since the TSP dissolution kinetics can vary, three cases were examined. In the first, the TSP was added to the solution before the Cal–Sil was added. This corresponds to instantaneous dissolution of the TSP and is clearly a bounding case. In the second case the TSP was added at a constant rate to the solution over a 1 h period. This is probably reasonably representative of most cases. In the third case the TSP was added at a constant rate over a 4 h period. This corresponds to the technical specification limit for the dissolution of TSP for most plants, and is taken as a lower bound on the TSP dissolution rate.

Tests were performed for Cal–Sil loadings of 1.5 and 0.5 g/l. The 1.5 g/l is probably an upper bound for the Cal–Sil loading. The 0.5 g/l is a more representative condition for most plants that use Cal–Sil. The Cal–Sil and TSP were added to a base solution with 2800-ppm-B and 0.7-ppm-Li. The total TSP added was equivalent to 3.4 g/l (264 ppm) and would be expected to give a pH of 7.14 without considering the pH changes due to Cal–Sil dissolution. As noted three different rates of TSP addition were considered. As shown in Table B5, a Cal–Sil loading of 1.5 g/l and a TSP addition of 264 ppm is the nominal boundary between solutions with excess PO_4^{-3} and those with excess Ca if $Ca_3(PO_4)_2$ is taken as the precipitation product.

Table B5. Calculated concentration of Ca and P forming $Ca_3(PO_4)_2$

Cal–Sil Loading, (g/l)	ppm-Ca fully dissolved	ppm-P to exhaust Ca	ppm-P in solution	solution ppm-Ca	Note
0.0	0.0	0.0	*264.20	All the Ca in the	TSP pH=7.14
0.1	34.6	17.8	246.4	$Ca_3(PO_4)_2$	TSP excess condition
0.5	172.8	89.0	175.2	Sediment	
1.5	512.8	264.2	0.00	0.00	TSP pH = 7.14

The tests results for the three TSP addition rates are shown in Table B6. Because of the difficulties in obtaining a sample while simultaneously adding TSP, the sampling was done at times sampling times 5-10 min, 30-min, 160-min, 24-h, 3-days, 5-days after the addition of TSP was completed. Thus for the cases when the TSP was added over 1 and 4-h intervals, 1 or 4 h would have to be added to the reported sampling time to get the actual time the Cal–Sil has been in the solution.

The samples were taken from the supernate solution. A 5-ml syringe was used to take a 2-ml sample of solution. In order to avoid including fine particles of pulverized Cal–Sil and/or of the reaction product, i.e., $Ca_3(PO_4)_2$ in the samples, the samples were filtered.. The tip of the syringe was wrapped with three layers of filter paper (1-cm x 1-cm #42 commercial filter paper). Platinum wire was wrapped about the filter paper to hold it in place. Because of the flow resistance introduced by the filter paper, it could take 2-3 min to obtain a sample.

Table B6. Compiled results of the elemental ICP-analysis for the supernate/filtered solutions for the three procedures of the TSP buffering during the 1.5-g CalSi/l leaching process.

TSP dissolution	Time (h)	pH (RT)	Elemental ICP-analysis (mg/l)					
			Ca	**P**	**K**	**Si**	**Na**	**Ca_{est}**
I "Instantaneous"	0.08	7.04	38.5	263	17.0	23.3	536	66
	0.50	7.17	24.6	252	4.44	24.4	554	74
	2.67	7.38	15.6	232	3.63	36.0	549	103
	24.50	7.24	7.91	165	6.58	59.7	534	225
	71.25	7.33	4.11	135	7.5	66.9	557	280
	118.5	7.48	3.29	132	4.29	68.2	567	285
II "1-h dissolution"	0.08	6.83	58.4	64.6	<2.5	20.8	159	470
	0.50	6.79	54.4	66.3	<2.5	22.0	168	463
	2.67	7.10	10.5	131	2.74	25.1	357	294
	23.50	7.10	4.68	103	4.76	45.6	382	342
	70.25	7.15	<2.5	67.1	5.55	62.1	405	407
	119.5	7.26	<2.5	56.8	3.59	65.2	395	427
III "4-h dissolution"	0.08	7.12	18.7	102	6.29	26.2	289	358
	0.50	6.85	14.4	104	32.5	27.6	295	350
	2.67	6.92	6.29	95.0	8.09	30.1	297	359
	19.50	6.99	4.77	66.7	4.75	42.0	292	413
	66.75	7.10	<2.5	36.0	4.81	59.7	327	467
	115.5	7.25	3.13	22.0	3.50	64.5	331	497

The difference between the total added 264-ppm-P and concentrations P in the solution gives the amount of P into the sediment. The measured Ca is not the total Ca that has been leached from the Cal-Sil; since most of the dissolved Ca precipitates out. The total dissolved Ca can be estimated if it is assumed that the precipitate is $Ca_3(PO_4)_2$.

Figure B12(a) shows the elemental wt. % in the sediments for the procedure-I, II, and III. For procedure-I, the ratio of P relative to the Ca and Si is smaller than for procedures II and III. This is due to Cal–Sil residue. This residue visibly colors the sediment as shown in Fig. B13. The molar ratio of Ca/P in the resulted sediments for procedures I, II, and III is shown in Fig. B12(b). The excess of the ratio value 1.5

[status of the P in the sediment as $Ca_3(PO_4)_2$ i.e., R = 1.5] is probably due to Cal–Sil residue. The ratio is closest to 1.5 for procedure III which would be expected to have the most complete dissolution.

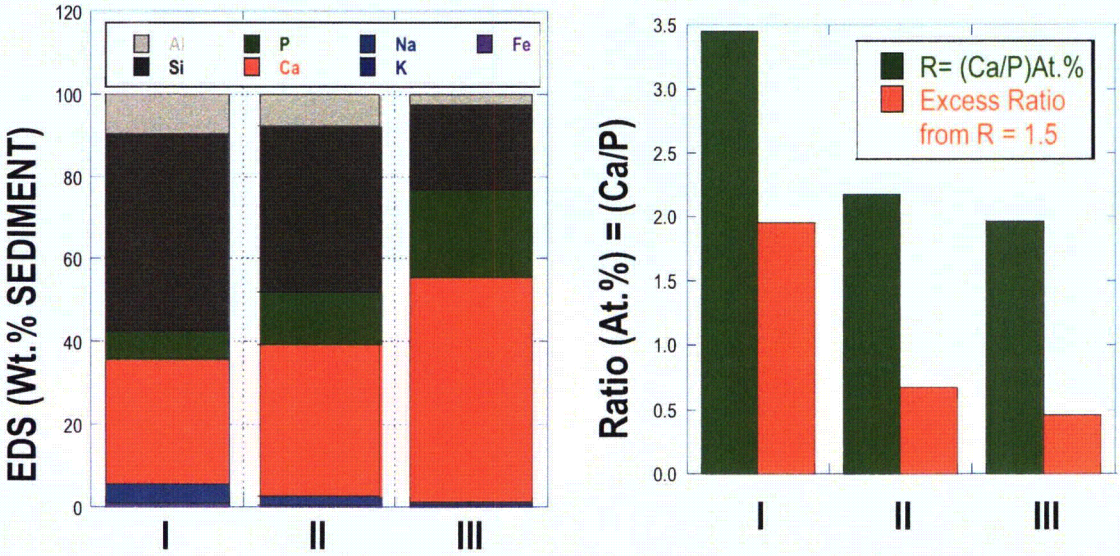

Figure B12 (a) Elemental wt. % in the sediments for the I, II, and III. (b). Molar ratio of Ca/P in the sediments for the I, II, and III.

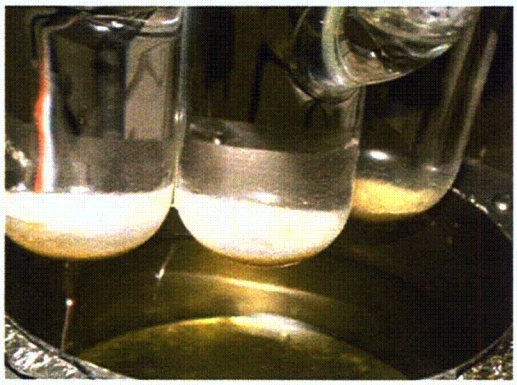

Figure B13.
Precipitates from the three procedures: Proc-III (lef: white ppt) , II (middle white ppt), and I (right side mostly yellowish) photo taken at t time 239-h.

The total weight of the recovered sediment is shown in Table B7 and compared to the initial weight of the Cal–Sil added to the solutions.

Table B7. Weight measurement for the dried sediments for the residue from Proc-I, II, and III for the 1.5-g Cal–Sil/l loadings.

Procedure	Cal–Sil initial Wt. (g)	Final collected sediment Wt.(g)	Wt. Yields (%) = Wt(f)/Wt(i)
I	0.225-g	0.195-g	87%
II	0.225-g	0.308-g	137%
III	0.225-g	0.272-g	121%

0.5-g Cal–Sil/l + 3.4-g TSP/l with three procedures; I, II, & III: The results from Cal–Sil leaching tests performed with 0.5-g Cal–Sil/l addition of 3.4-g TSP/l with three procedures; I, II, & III are given in Table B8 and in illustrated in the Fig. B14.

Table B8. Compiled results of the elemental ICP-analysis for the supernate/filtered solutions for the three procedures of the TSP buffering during the 0.5-g CalSi/l leaching process.

TSP buffering procedure	Time (h)	Elemental ICP-analysis (mg/l)				
		Ca	P	K	Si	Na
	0.08	9	250	7	7	598
	0.50	9	241	7	9	585
I	2.67	10	223	7	20	594
"Instantaneous"	24.00	4	208	7	36	600
	72.00	3	198	7	42	579
	120.00	3	199	7	42	577
	0.08	14	211	7	9	512
	0.50	14	249	7	12	618
II	2.67	13	237	7	20	620
"1-h"	23.00	7	222	7	37	627
	71.00	4	216	7	45	631
	119.00	4	225	7	47	642
	0.08	21	230	7	22	585
	0.50	18	229	7	24	600
	2.67	7	212	7	28	582
III	20.00	4	201	7	37	583
"4-h"	68.00	3	206	7	44	600
	116.00	4	203	7	46	601

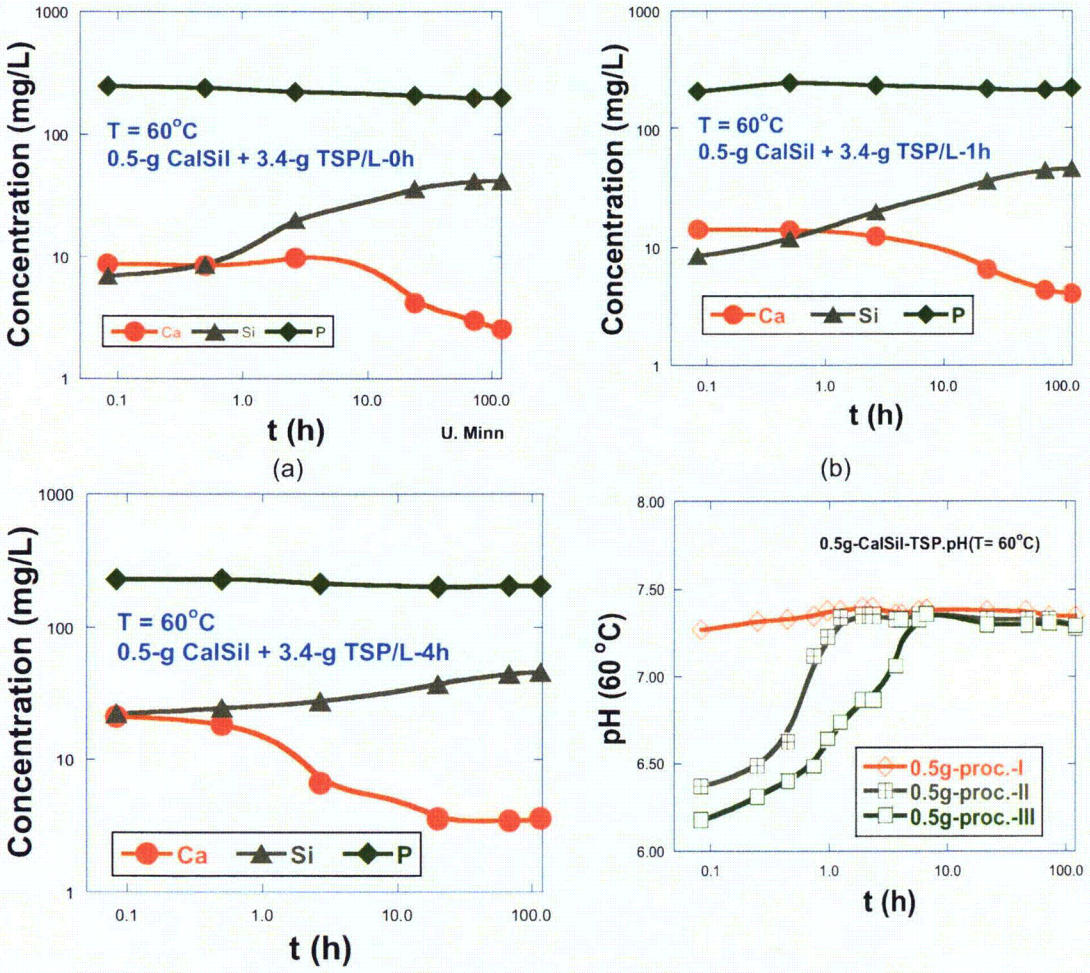

Figure B14. Concentration of the element vs. time for the Cal–Sil loading of 0.5-g Cal–Sil/l process at 60°C added total 3.4-gTSP/l as (a) procedure-I, t = 0, (b) procedure-II for t = 1-h, (c) procedure-III for t = 4-h, and (d) the pH (60°C) vs. time for the three procedures.

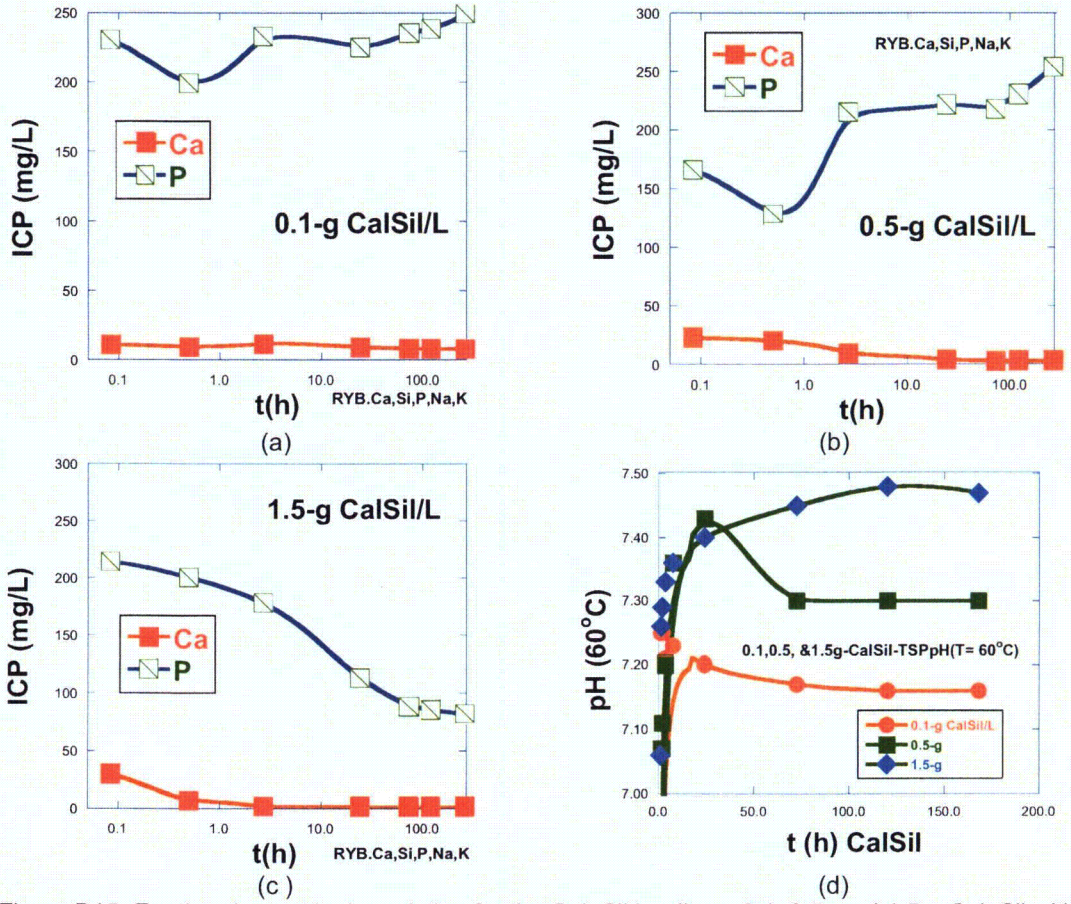

Figure B15. For the element in the solution for the Cal–Sil loadings, 0.1, 0.5, and 1.5-g Cal–Sil with 3.4-g TSP/l and pH (60°C) vs. time for the three procedures Loading of 0.1, 0.5, and 1.5.

pH (60°C) vs .t for the progress [0.1, 0.5, and 1.5-g Cal–Sil with 3.4-g TSP/l: Figure B15 shows the result of the Cal–Sil leaching tests performed with 0.1, 0.5, 1.5-g Cal–Sil/l addition of 3.4-g TSP/l vs. time.

Table B9. Measured pH values at 60°C in-situ dissolution tests, and pH (RT) for the ICP-samples

Time (h)	pH @60°C, in-situ			pH (RT) for ICP-samples		
	0.1g	0.5-g	1.5-g	0.1g	0.5-g	1.5-g
0.87	5.82	6.08	6.39			
1.00						
1.05	6.95	6.99	7.06			
1.42	7.25	7.07	7.26	7.19	7.15	7.19
1.92	7.25	7.11	7.29	7.23	7.03	7.30
3.58	7.21	7.20	7.33			
7.58	7.23	7.36	7.36	7.24	7.29	7.42
24.08	7.20	7.43	7.40	7.23	7.37	7.45
72.5	7.17	7.30	7.45	7.23	7.38	7.50
120.0	7.16	7.30	7.48	7.20	7.32	7.48
168.0	7.16	7.30	7.47	7.18	7.23	7.49

1.5-g Cal–Sil Dissolution Tests T = 90°C procedures –I, II, and III: Figure B16 showed the results of the elemental ICP-analysis on the 1.5-g/l Cal–Sil dissolution for the I, II, and III procedures and pH (RT) vs. t , after TSP addition finished. The Na and Si concentrations are higher than that of the dissolution tests performed 60°C, but the Ca levels are lower.

The data from the small–scale dissolution tests at 90°C are summarized in Table B10. The Na levels are much higher than in the corresponding tests at 60°C, indicating more leaching of the Na from the Cal–Sil. The Ca in solution is lower reflecting the retrograde solubility of $Ca_3(PO_4)_2$. The measured P levels are, however, much higher than those at 60°C indicating that not as much $Ca_3(PO_4)_2$ has formed, which implies that less Ca has leached from the Cal–Sil at the higher temperature.

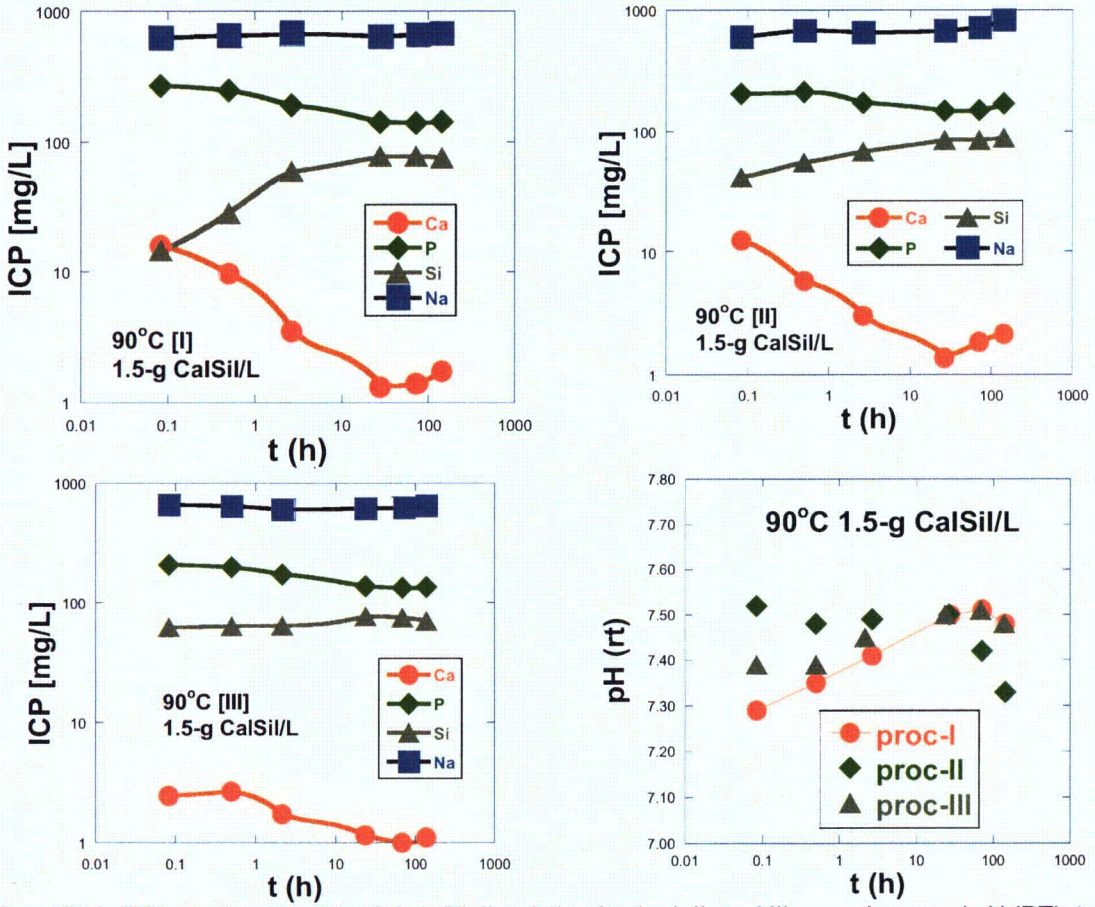

Figure B16. ICP-result on the 1.5-g/l Cal–Sil dissolution for the I, II, and III procedures and pH (RT). t = after TSP addition finished.

Table B10. Summary of results for the small–scale dissolution tests at T= 90°C.

Test series	Time (h)	pH (RT)	Ca (mg/l)	P (mg/l)	Si (mg/l)	Na (mg/l)	Cal–Sil (g/l)	Ca equiv (mg/l) $(Ca_3(PO_4)_2)$	Ca equiv (mg/l) $Ca_{10}(PO_4)6(OH)_2$
I TSP is added before the Cal–Sil is introduced	0.08	7.29	16	272	15	633	1.5	10	11
	0.50	7.35	10	250	28	658	1.5	52	58
	2.67	7.41	3	193	59	671	1.5	163	181
	24.50	7.50	1	143	77	648	1.5	259	288
	71.25	7.51	1	141	77	666	1.5	263	292
	119.00	7.48	2	144	75	686	1.5	257	286
II TSP metered over an hour after the Cal–Sil is added	1.08	7.52	13	206	41	599	1.5	137	153
	1.5	7.48	6	213	55	678	1.5	124	138
	3.67	7.49	3	173	68	651	1.5	201	224
	25.5	7.50	1	149	85	673	1.5	248	275
	72.25	7.42	2	150	85	718	1.5	246	273
	120	7.33	2	171	88	829	1.5	205	228
III TSP metered over a 4 hour period.	4.08	7.38	2	207	62	663	1.5	135	151
	4.5	7.38	3	197	63	647	1.5	155	172
	6.67	7.44	2	172	64	608	1.5	203	226
	28.5	7.45	1	136	76	619	1.5	273	303
	75.25	7.45	1	133	75	625	1.5	279	310
	123	7.49	1	135	70	650	1.5	275	305

Appendix C Surrogates for the ICET-1 environment

C1. Aluminum nitrate

Aluminum nitrate solutions with dissolved Al levels of 350 ppm, 150, ppm, and 50-ppm have been investigated. The solutions were prepared by dissolving commercial aluminum nitrate, $Al(NO_3)_3 \cdot 9H_2O$ powder in solutions with 2800 ppm B added as boric acid and NaOH additions to make the pH = 10 at room temperature. Table C1 shows the amount of aluminum nitrate added to each solution and the appearance of the solutions after mixing as room temperature.

Although the 350-ppm-Al solution was not fully dissolved at room temperature, virtually all (~95%) the emulsion disappeared after the solution was reheated to 60°C. Figure C1a shows the appearance of the solution at room temperature; Fig. C1b shows the solution at 96.3°C; and Fig. C1c shows the solution after cooling to 28.0°C. A more complete sequence of images documenting the heat–up and cool–down process is given in Appendix D. The relatively high degree of redissolution suggests that the emulsion is primarily an amorphous $Al(OH)_3$ solid, since the crystalline forms have very low solubility and would be much less likely to redissolve.

Table C1. Preparation and the visual observations of the 50, 150, and 350-ppm-Al solutions prepared from aluminum nitrate, $Al(NO_3)_3 \cdot 9H_2O$.

Solution	Al (ppm)	Vol (ml)	*Wt. (g)	Visual observations
A	50	176	0.1	Initially gelatin like emulsion was revealed, but solution becomes cleared after 2-h later
B	150	126	0.3	At room temperature bottom 10 % emulsion
C	350	122	0.6	At room temperature bottom 30 % emulsion, but at 93°C the solution was totally clear.

*$Al(NO_3)_3$-$9H_2O$ [MW = 375.13g for $Al(NO_3)_3$-$9H_2O$]

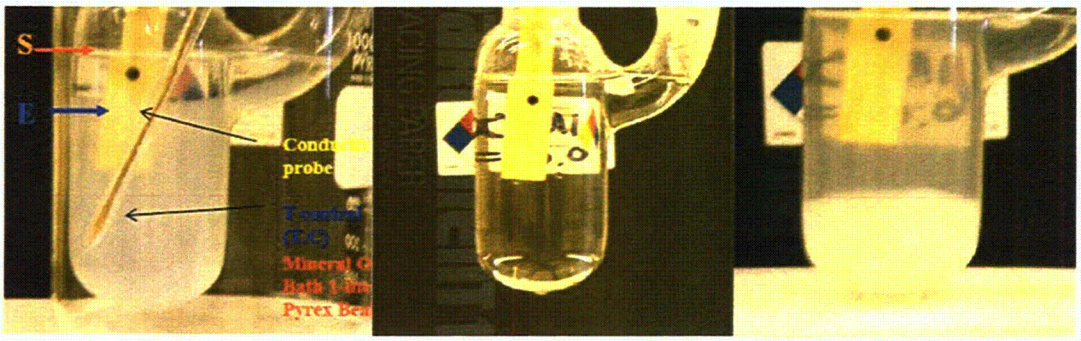

(a) (b) (c)

Figure C1. 375-ppm-Al solution. (a) at 20.5°C (room temperature) 10-min after mixing. Note: S = Solution level, E = Emulsion level; (b) heated up to 96.3°C, t = 53 min after mixing; and (c) cooled down to 28.0°C , t = 247 min after mixing.

The electrical conductivity was measured as a function of temperature and concentration to characterize ionic behavior. The temperature dependence of the conductivity is shown in Fig. C2. The conductivity decreases with increasing Al concentration. This suggests that the conduction is mostly due to Na^+ and OH^- ions, and the OH^- concentration is decreasing as more $Al(NO_3)_3$ is added.

$$4NaOH = 4Na^+ + 4OH^- \quad (C1)$$

$$Al(NO_3)_3 = Al^{+3} + 3NO_3^- \quad (C2)$$

$$4NaOH + Al(NO_3)_3 = Al(OH)_4^- + 4Na^+ + 3NO_3^- \quad (C3)$$

The highly conductive hydroxyl ions are captured by the formation of $Al(OH)_4^-$, which are lower mobility anions compared with the OH^- ions. The measured solution pH values after the additions of the aluminum nitrate were 10.06 for 50-ppm Al , 9.96 for 150-ppm Al, and 9.72 for 350-ppm-Al. The trend in the pH values is consistent with Eq. (C3).

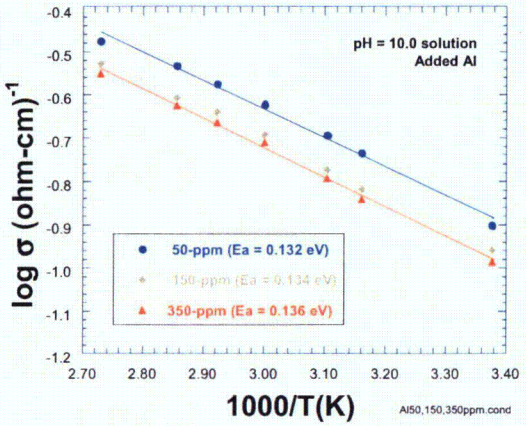

Figure C2. Electrical conductivity vs. 1/T. for the pH = 10.0 solution added 50, 150, and 350-ppm of aluminum ions.

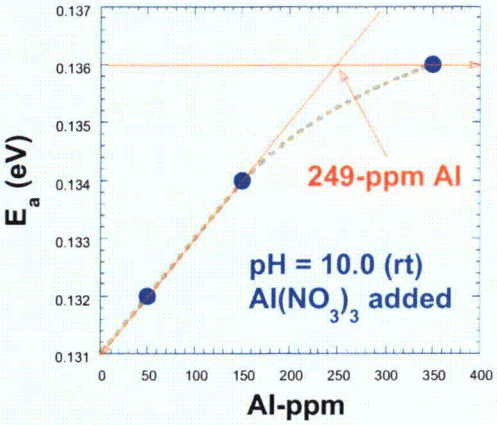

Figure C3. Activation energy, E_a vs. Al-ppm in the pH = 10.0 solution added $Al(NO_3)_3$.

The activation energy, E_a vs. dissolved Al-ppm is shown in Fig C3. The 350-ppm does not behave as an ideal solution, i.e., it deviates from the linear behavior that characterizes the lower concentration solutions. This indicates that the solution may not be dissociating completely at these concentrations.

Figure C4a compares the viscosities of a 370-ppm-Al solution and ultra–high–purity (UHP) water as a function of temperature. Figure C4b shows the viscosities of solutions with 50, 150, and 350-ppm dissolved Al and solutions from two head loss tests. The viscosity measurements were performed using an Ostwald-viscometer. The measured viscosity for the 370-ppm-Al solution is somewhat greater than the UHP water. The results shown in Figure C4 are for well mixed solutions. Separating off the supernate, and then measuring the viscosity of the remaining solutions gives viscosity values approximately twice those shown in the figure.

The temperature dependence of the viscosity can be described in terms of an activation energy of 0.139 eV. This is close to the observed value for the activation energy for the conductivity, 0.136 eV, as shown in Figure C2. The activation energy for the conductivity is related to the transport of mobile ionic

species. The temperature dependence of the viscosity could also be related to an energy barrier for transport.

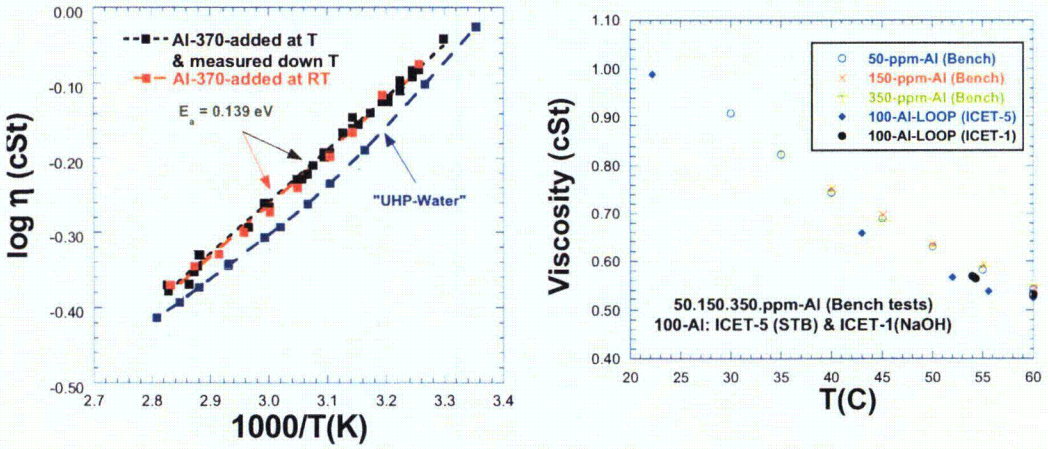

((a) (b)

Figure C4. Temperature dependence of viscosity (η): (a) Black and red symbols are for solutions with 370 ppm Al, and the blue symbols for the UHP-water, and (b) Viscosity (η) of 50, 150, and 350-ppm-Al bench top solutions , and and 100-ppm-Al solutions samples from the loop during head loss tests for the ICET-5 and ICET-1 environments.

Figure C5 shows the settlement of the Al emulsion. The emulsion was allowed to form, then the solution was shaken to homogenize it and then allowed to settle. The volume of solution in which the emulsion was visible was monitored as a function of time.

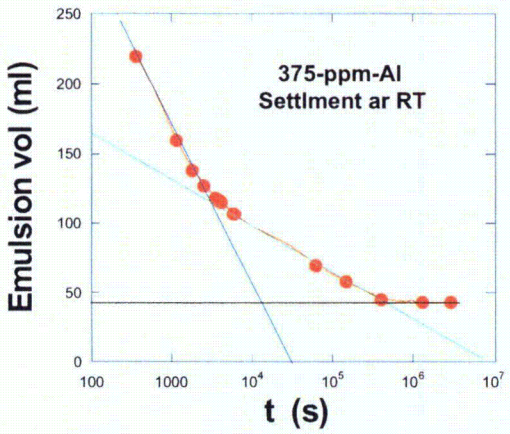

Figure C5.
Volume of the emulsion settled in the 375-ppm-Al solution as a function of time at RT. The total solution volume is 230 ml.

C2 Sodium Aluminate

The use of aluminum nitrate to create surrogate solutions has some disadvantages. It introduces a species (nitrate) that is not typically present in the sump environment, and tends to drive the pH down. A peer reviewer (C. Delegard, PNNL) suggested investigating the use of sodium aluminate ($NaAlO_2$) to create the surrogate solutions. This would introduce no new species, would not tend to decrease the pH, and

better mimics the actual corrosion process since the formation sodium aluminate ($NaAlO_2$) is probably an intermediate step in the actual dissolution of metallic Al in a NaOH environment.

To create a surrogate using sodium aluminate ($NaAlO_2$), 250-ml of boric acid solution with LiOH [pH(RT) = 5.01] was heated in a flask to 60°C and an appropriate amount of $NaAlO_2$ to reach the target concentration of Al was added. The solution pH was increased to 7.49 at 60°C by the addition of the $NaAlO_2$. The $NaAlO_2$ was not fully dissolved. The solution was kept overnight at 60°C. Overnight, the pH increased to 7.54, but the sediment was still not fully dissolved. NaOH was added incrementally to increase the pH. The appearance of the solution during the test is described in Table C2, and shown in Fig. C6. The solution become completely clear at pH = 9.54. However, more NaOH was added to increase the pH to 10.0.

Table. C2. Visual observation and the pH variation during the NaOH additions: 375-ppm-Al solution made by adding $NaAlO_2$ in the $B(OH)_3$ + LiOH solution 250-ml.

Weight (g)	pH at 60°C	Solution state
0	5.01 (rt)	Only $B(OH)_3$ + LiOH
0	7.23	200-ppm-Al/ Not dissolved
0	7.49	375-ppmAl/ Not dissolved
0	7.54	After overnight 375-ppmAl/ Not dissolved
0.096	7.55	Not dissolved
0.194	7.77	"
0.983		"
1.081	8.93	Entire solution is slightly cloudy
1.278	9.00	Entire solution is cloudy
1.475		"
1.574	8.91(?)*	Top cloud and bottom totally clear
1.771	9.54**	Still cloud left
1.968	9.54-9.57	Solution much more clear
2.165	9.55-9.75	"
2.263		"
2.460		"
2.559	9.75	Solution clear
2.855	10.0	"

*Note: pH monitored at the top 20%. The solution separated; the top 60% was slightly cloudy, and at the bottom 40% was totally clear. The solution was shaken thoroughly before proceeding.
**Note: Solution totally clear, but NaOH was keep adding to adjust the pH = 10.0

375-pm-Al by adding $NaAlO_2$
Solution cloudy and undissolved sediment at the bottom

pH = 7.54 (60°C)
time = 0 min

Relative uniform cloudiness
pH = 8.93 (60°C)
time = 22-min

All clear
pH = 10.0 (60.6°C)
time = 120-min

Figure C6. Visual and pH changes for the 375-pm-Al dissolution of $NaAlO_2$ vs. addition of NaOH at 60°C.

The solution was then cooled. It remained clear down to room temperature as shown in Fig C7. After over 5-days at RT , the solution was still clear, but some sediment could be seen at the bottom of the flask as shown in Fig. C8.

Figure C7. $NaAlO_2$ solution at T = 22.9°C, time = 450-min

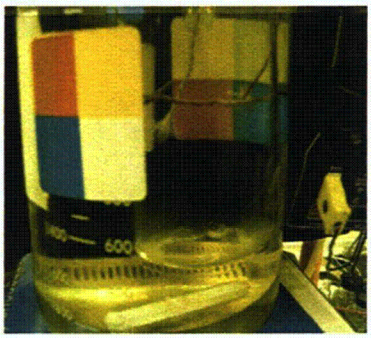

Figure C8. $NaAlO_2$ solution after over 5-days room temperature. A ring of white sediment is seen at the bottom. The sediment forms a ring because of the magnetic stirring.

Since the behavior of the system is expected to be sensitive to pH, a new solution was prepared with a target pH of 9.5. Boric acid with LiOH (pH_{RT} = 5.01, 250-ml) solution was heated to 60°C and 0.28480-g of $NaAlO_2$ powder was added to obtain a 375-ppm Al solution (see Fig. C9). The flask with the test solution is located inside the mineral oil bath and the pH probe is located at the center of the flask and is submerged about 25%. The solution pH was adjusted to 9.50 at 60°C by adding NaOH (1.57375-g). The solution became totally clear at 60°C (see Fig. C10).

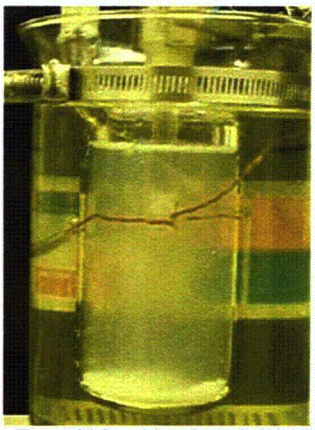

Figure C9. T = 60°C, pH = 9.5; 0.28480-g of $NaAlO_2$ equivalent to 375-ppm Al was added to B(OH)3 + LiOH base solution. Undissolved sediment remained at the bottom.

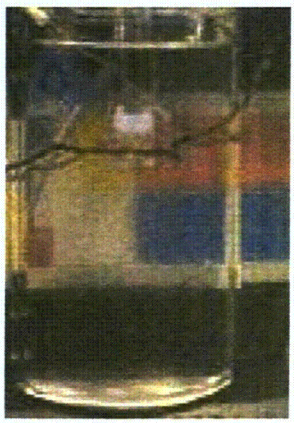

Figure C10. T = 60°C, pH = 9.5 for the 375-ppm Al. Test flask is inside the mineral oil bath. Backside color level indicates the solution is totally clear.

The solution was then cooled. The appearance of the solution during the cooling process is shown in Figs. C11–C15.

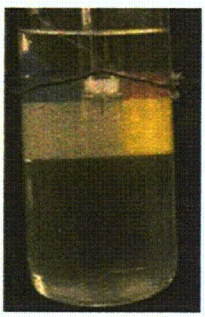

Figure C11. $NaAlO_2$ solution at 38.9°C, still clear. Cooling time = 90-min.

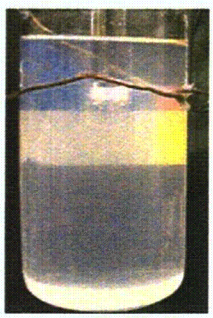

Figure C12. $NaAlO_2$ solution 22.4°C. Cooling time =270-min. Some cloudiness is visible.

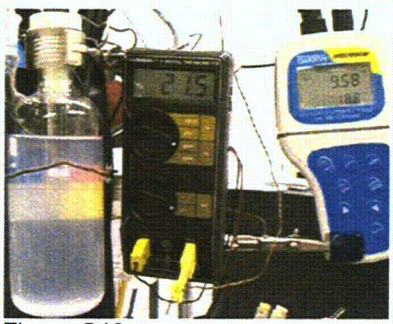

Figure C13. $NaAlO_2$ solution at 21.5°C Cooling time 273-min. Cloudiness is visible and pH has increased to 9.58.

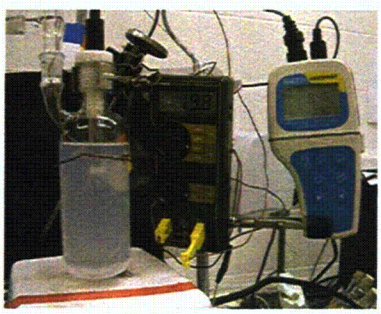

Figure C14. $NaAlO_2$ solution at 19.8°C. Cooling time 17-h. pH decreased to 9.46 (may be due to CO_2).

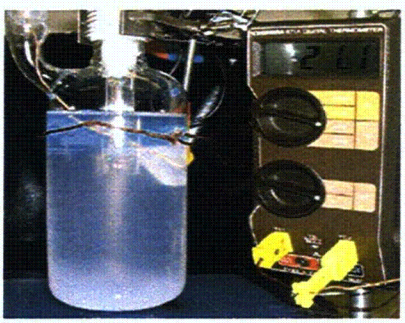

Figure C15. $NaAlO_2$ solution at RT after 46-h Emulsion fills 15% height at the bottom.

The process was repeated with a lower target pH of 9.3. Boric acid with LiOH (pH_{RT} = 5.01, 250-ml) solution was again heated to 60°C in the two port flask and 0.28480-g of $NaAlO_2$ powder was added to get 375-ppm Al. The solution pH was then adjusted to 9.28 at 60°C by adding NaOH (1.08112-g). The solution was initially cloudy (Fig. C16), but after about 60 min it became clear.

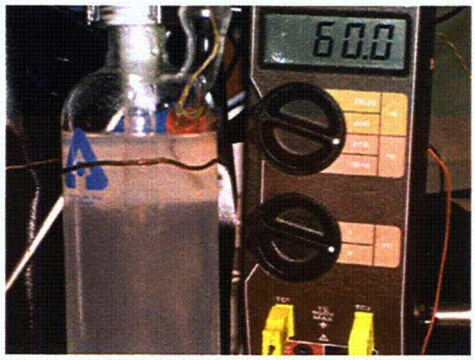

Figure C16.
$NaAlO_2$ solution at 60° pH = 9.28.

The solution was then cooled. Figure C17 showed the solution 17-h later at RT. The emulsion has settled, and represents about 15% of the volume. The emulsion was still very transparent with no solid sediment. The pH increased to 9.5. This increase in pH is expected as the aluminate ion dissociates to form $Al(OH)_3$, $Al(OH)_4^- = Al(OH)_3 + OH^-$. Figure C18. shows the solution 46-h later at RT. The emulsion cloud still occupies 15% height at the bottom there is little change in appearance.

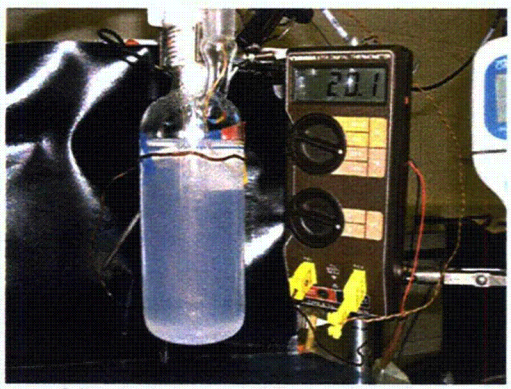

Figure C17. 17-h later at RT, a rather clear, transparent emulsion cloud occupies about 15% of the volume at the bottom of the flask.

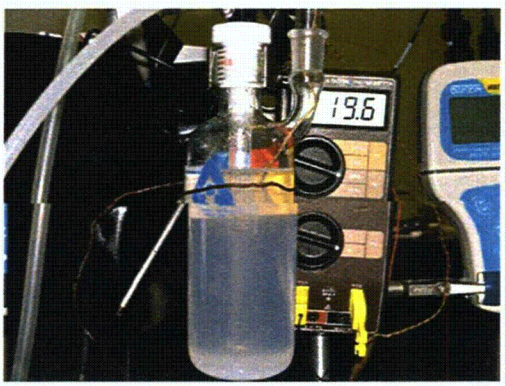

Figure C18. 46-h later at RT, the emulsion cloud still occupies about 15% of the volume and there is little change in appearance.

Figure C19 compares the concentration of Al vs. pH in the supernate solutions based on the results of the Inductively Coupled Plasma (ICP) analysis for the dissolved $NaAlO_2$ equivalent Al concentration of 375-ppm-Al. The measured results agree reasonably well with those expected assuming the soluble form is $Al(OH)_4^-$. The higher the pH, the higher is the Al in the supernate solution, i.e., the higher the solubility. Figure C20 shows the concentration of Al and B vs. pH for the 375-ppm-Al with dissolved $NaAlO_2$. The simultaneous decrease in concentration of both B and Al in the supernate solution with pH indicates that the B is incorporated in the emulsion along with A.

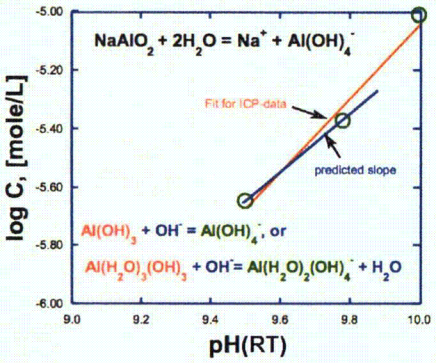

Figure C19
Concentration of Al vs. pH in the supernate solutions

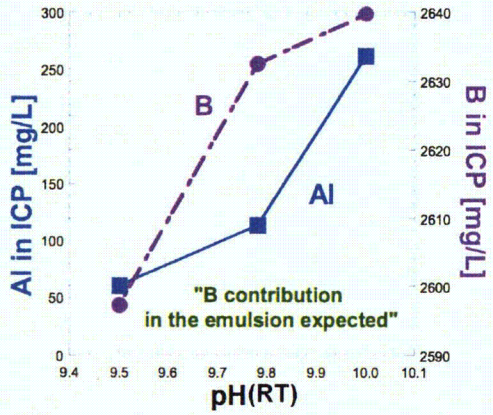

Figure C20.
Al and B vs. pH in the 375-ppm-Al with dissolved $NaAlO_2$ The simultaneous decrease in concentration with pH indicates that the B is incorporated in the emulsion along with Al.

The overall qualitative behavior of the 375-ppm-Al solution obtained by dissolution of $NaAlO_2$ is summarized in Table C3.

A qualitative comparison of the behavior and appearance of the precipitates in the sodium aluminate and aluminum nitrate solutions with the precipitate behavior observed in the ICET–1 test as described in Reference (2) led to the judgment that precipitates in the aluminum nitrate solutions better reflected the behavior of the precipitates in the ICET–1 test.

C3 Characterization of precipitates

Transmission electron microscopy (TEM) images were obtained from the precipitate from a 375-ppm-Al solution. The precipitate gel had been stored in a closed container for about 6 months before the images were taken. The gel was rinsed in UHP water. A small portion of the gel (≈ 0.3 g) was mixed with 250-ml UHP water. The rinsed sediment was place on carbon film for TEM analysis. The results are shown in Figure C21. The particles typically have chunky rectangular or triangular shapes and are 0.5–1 μm in size. Energy dispersive x–ray spectroscipy (EDS) analysis of the particles shown in Fig. C22 showed the particles are mostly Al [90.34 wt (89.40 at) %] with 6.78 wt (7.87at.) % Na, and 2.88 wt. (2.74 at) % Si.

Table C3. Behavior of 375-ppm-Al solution from dissolution of $NaAlO_2$ with pH = 10.0, 9.5, and 9.28

pH at 60°C	Note
5.01 (rt)	Base solution of current task [$B(OH)_3$ + LiOH]
7.54	Only for the 375-ppm-Al dissolution of $NaAlO_2$. A large pile of sediment present at the bottom of the test flask after adding equivalent 375-ppm-Al.amount of $NaAlO_2$ in the time between 0 and 17-h period
9.28	Little bit cloudiness at all temperatures, but becomes a little more transparent at RT with the transparent particles sediment at the bottom.
9.50	Clear at 60°C, but becomes little cloudiness was shown at RT with a very pale cotton pad shape emulsion arraying at the lower part of the solution.
10.0	Clear at all temperatures. But 5-days later, a very small amount of white particle sediment was shown. But none of the cloudiness was shown in the solution at all.

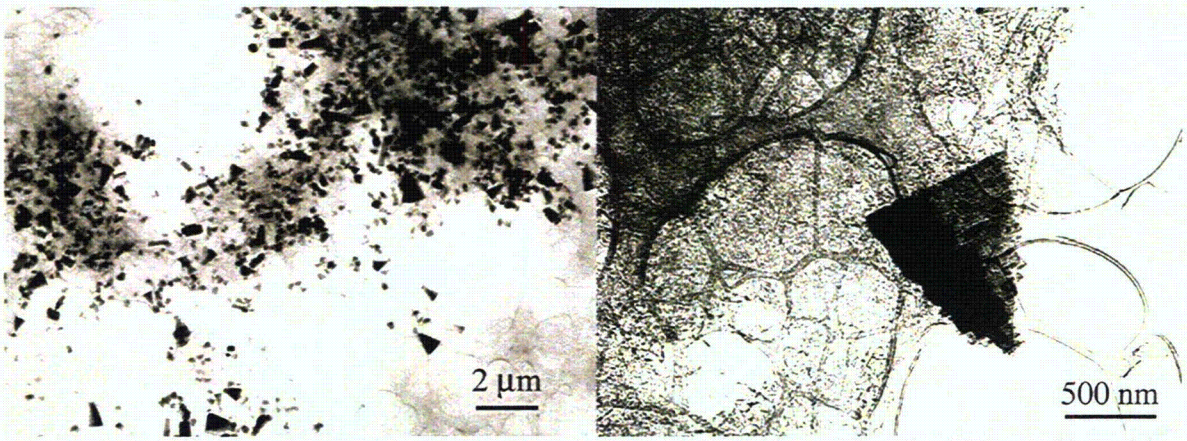

Figure C21. TEM views for the particles (black) on the carbon film collected from the 375-ppm-Al emulsion after rinse with UHP water.

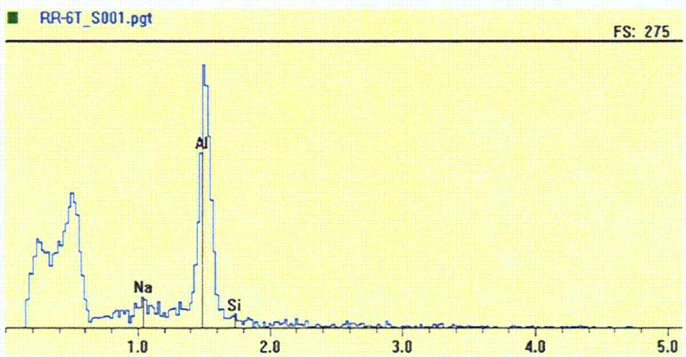

Element	Wt%	At%
Na	6.78	7.87
Si	2.88	2.74
Al	90.34	89.40

Figure C22. EDS chemical analysis of the $Al(OH)_3$ precipitate after rinsing with UHP water.

The shapes of the particles suggests that the material primarily crystalline, although no conclusive electron diffraction patterns were obtained in the TEM analyses. This is consistent with the relative insolubility of the aged product. At a given pH, the solubility of a crystalline phase like gibbsite is smaller than that of the amorphous phase by a factor of about 500. Freshly precipitated material will quickly redissolve if the temperature of the solution is raised to 60°C. The aged material shows little tendency to redissolve if the temperature is increased.

To try to visualize better the nature of the emulsion, a small portion of the fine emulsion from a 100-ppm-Al solution was quenched at liquid-nitrogen (LN) temperature. To quench the sample, the scanning electron microscopy (SEM) sample stage was cooled to LN temperature. A very small drop of the solution was quickly rubbed onto the cooled sample stage. It immediately started vacuum drying at LN temperature. These conditions were intended to minimize the tendency for the particles to migrate or coagulate. Figure C23 shows SEM pictures of the vacuum dried emulsion particles on the Au-substrate. The emulsion particles are evenly dispersed, and the clusters look elongated (0.2 x 0.5-2 μm size) in the enlarged view. EDS for a single particle on the Au foil (without washing of the emulsion with UHP water) gives 21.01 wt (24.47at.) % Na, 73.26 wt.(69.84at) % Si, and 5.73 wt (5.69 at)% Al.

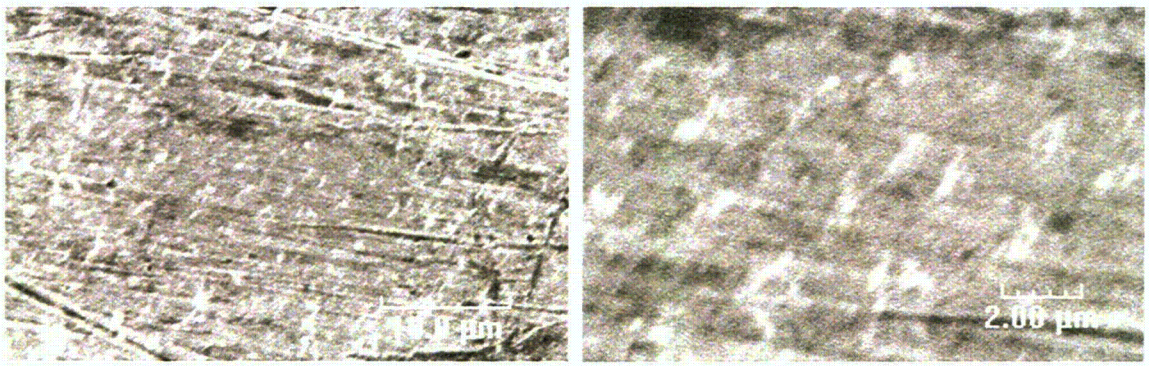

Figure C23. SEM pictures of the vacuum dried emulsion particles on the Au-substrate.

Appendix D Visual Observations of a 375-ppm-Al solution

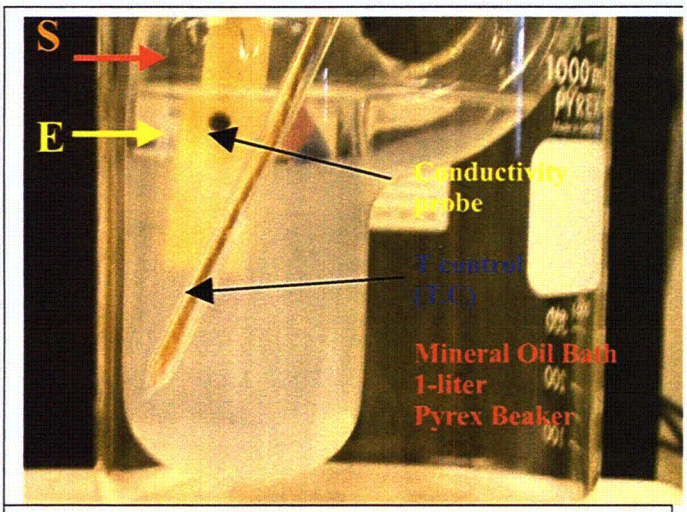

Figure D1

T= 20.5°C (RT)
t = 10-min after mixing 123.0 grams of pH =10.0 solution with 0.60 gram of $Al(NO_3)_3 \times 9H_2O$.

σ = 126.9 μ-MHO

Note: S = Solution level
E = Emulsion level
*Before adding the mineral oil into the beaker.

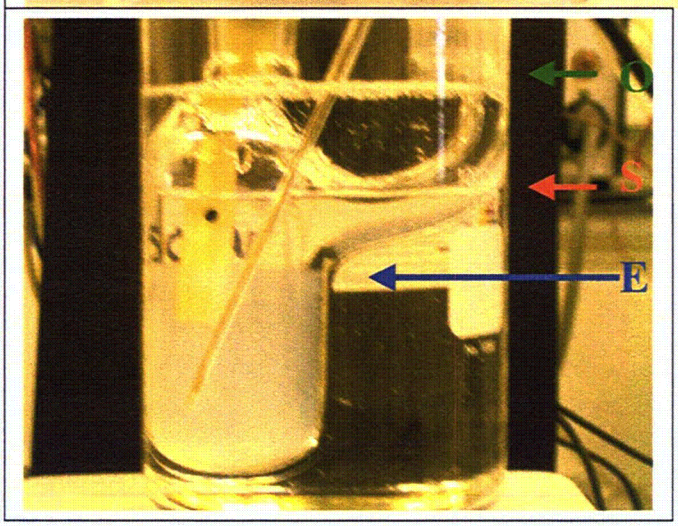

Figure D2

T= 21 °C (RT)
t = 12 min after mixing 123.0 grams of pH =10.0 solution with 0.60 gram of $Al(NO_3)_3 \times 9H_2O$.

σ = 127.5 μ-MHO

Note: O = Oil bath level
S = Solution level
E = Emulsion level
*After adding the mineral oil for the oil bath.

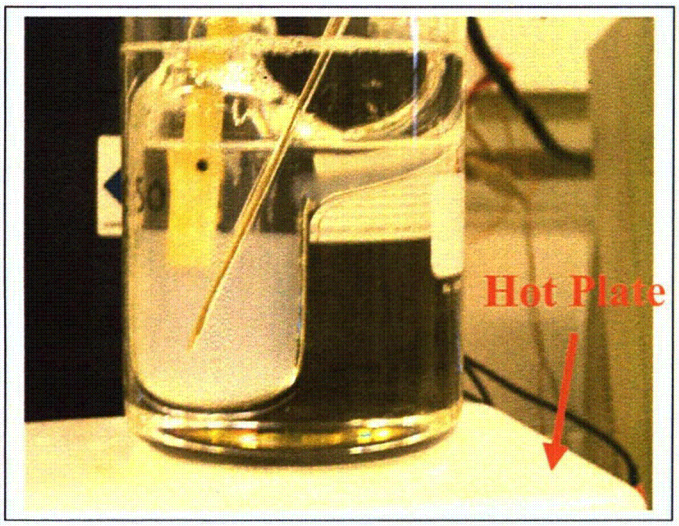

Figure D3

T= 21 °C (RT)
t = 14 min after mixing 123.0 grams of pH =10.0 solution with 0.60 gram of $Al(NO_3)_3 \times 9H_2O$.

σ = 127.7 μ-MHO

Note: Emulsion level down

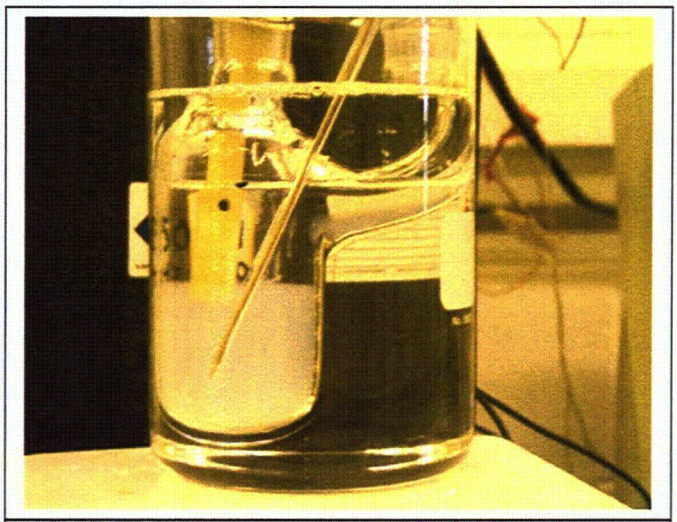

Figure D4

T= 21 °C (RT)
t = 20 min after mixing 123.0 grams of pH =10.0 solution with 0.60g ram of $Al(NO_3)_3 \times 9H_2O$.

σ = 128.3 μ-MHO

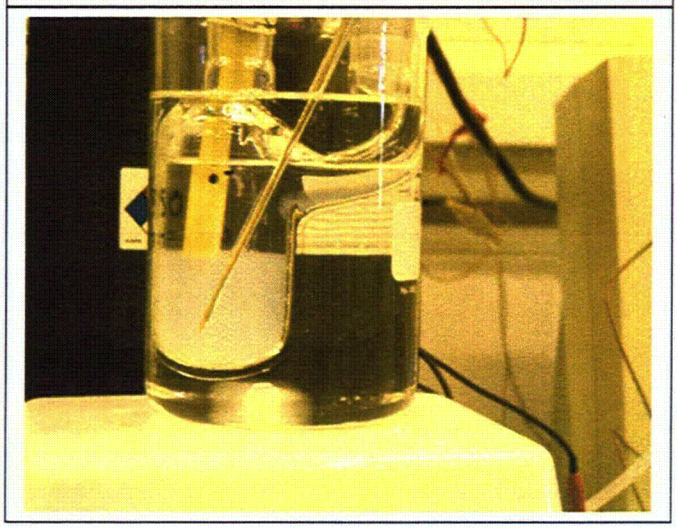

Figure D5

T= 21 °C (RT)
t = 21 min after mixing 123.0 grams of pH =10.0 solution with 0.60 gram of $Al(NO_3)_3 \times 9H_2O$.

σ = 128.6 μ-MHO

Note: Magnetic stirring bar inserted into the oil bath

Figure D6

T= 21.8 °C (RT)
t = 27 min after mixing 123.0 grams of pH =10.0 solution with 0.60 gram of $Al(NO_3)_3 \times 9H_2O$.

σ = 133.5 μ-MHO

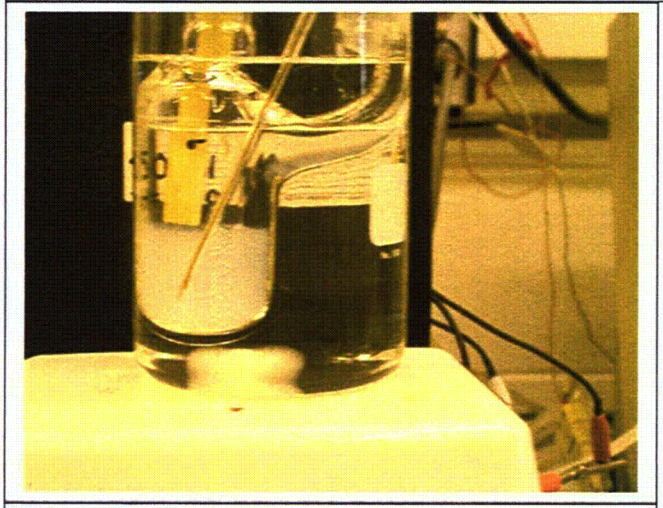

Figure D7

T= 30.1 °C
t = 30 min after mixing 123.0 grams of pH =10.0 solution with 0.60 gram of $Al(NO_3)_3 \times 9H_2O$.

σ = 164.7 μ-MHO

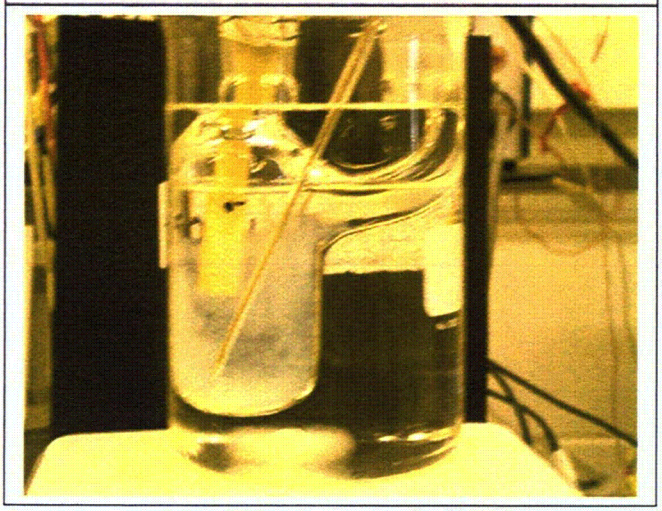

Figure D8

T= 44.1°C
t = 32-min after mixing 123.0 grams of pH =10.0 solution with 0.60 gram of $Al(NO_3)_3 \times 9H_2O$.

σ = 215 m-MOH

Note: Emulsion is dispersed by convection of solution

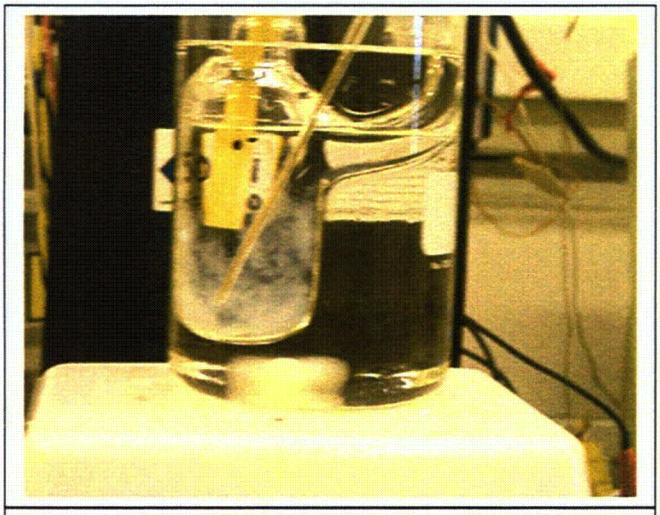

Figure D9

T= 51.2°C
t = 32-min after mixing 123.0 grams of pH =10.0 solution with 0.60 gram of $Al(NO_3)_3 \times 9H_2O$.

σ = 239 μ-MHO

Note: Scattered emulsion cloud appears to be redissolving.

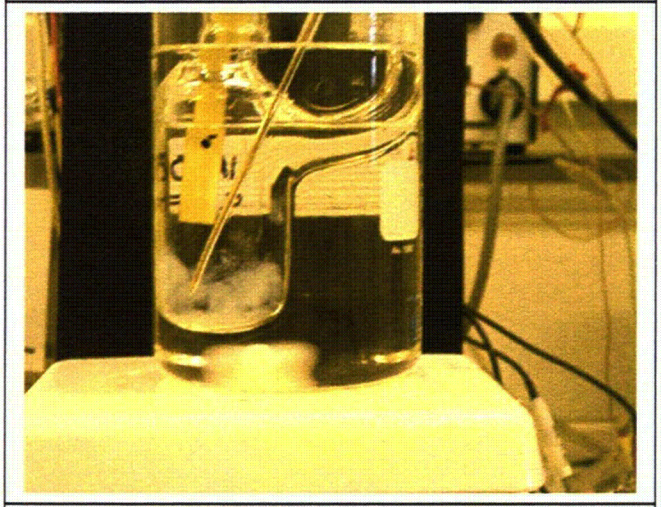

Figure D10

T= 63°C
t = 34 min after mixing 123.0 grams of pH =10.0 solution with 0.60 gram of $Al(NO_3)_3 \times 9H_2O$.

σ = 270 μ-MHO

Note: Emulsion cloud becomes less visible. Solution volume expands with increasing temperature (black dot level at the rt)

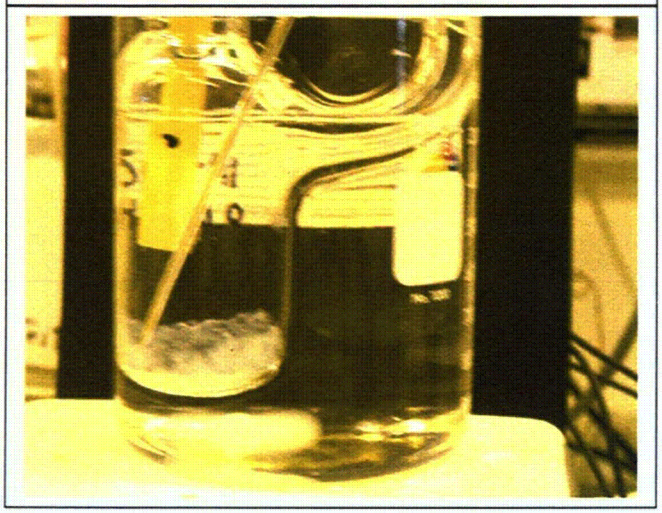

Figure D11

T= 68.3°C
t = 37 min after mixing 123.0 grams of pH =10.0 solution with 0.60 gram of $Al(NO_3)_3 \times 9H_2O$.

σ = 283 μ-MHO

Note: Emulsion continues to disappear but some sediment is evident. Many very tiny bubbles (the 0.1 mm dia. bubbles are not visible in the photo) were generated inside the emulsion; and traveled upward.

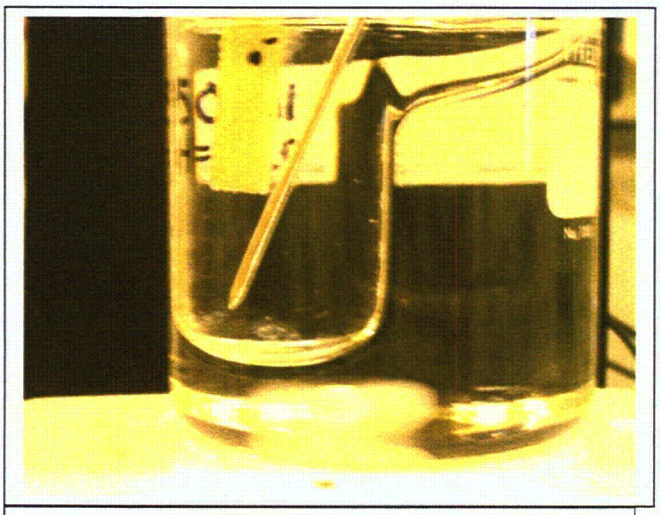

Figure D12

T= 77.2°C
t = 39 min after mixing 123.0 grams of pH =10.0 solution with 0.60 gram of $Al(NO_3)_3 \times 9H_2O$.

σ = 283 μ-MHO

Note: Emulsion cloud has almost disappeared except for a small amount of sediment.

Figure D13

T= 79.5°C
t = 39 min after mixing 123.0 grams of pH =10.0 solution with 0.60 gram of $Al(NO_3)_3 \times 9H_2O$

σ = 306 μ-MHO

Note: Emulsion cloud has almost disappeared, except for 0.5 x 0.5 x 0.12 cm volume of sediment left at the bottom of the flask.

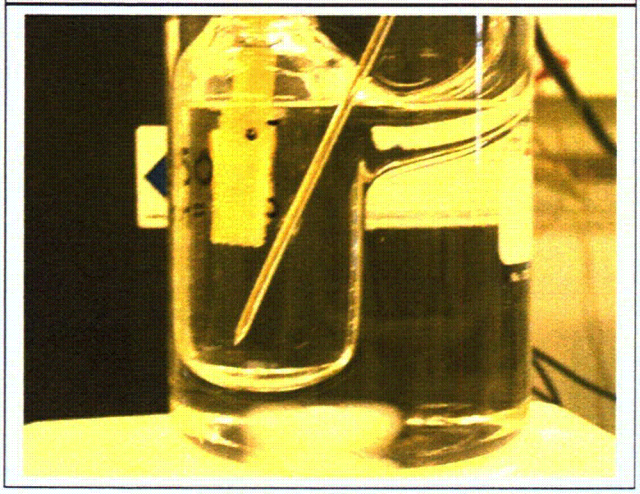

Figure D14

T= 81.4°C
t = 42 min after mixing 123.0 grams of pH =10.0 solution with 0.60 gram of $Al(NO_3)_3 \times 9H_2O$.

σ = 307 μ-MHO

Note: Emulsion cloud has almost disappeared, except for 0.5 x 0.5 x 0.12 cm volume of sediment left at the bottom of the flask.

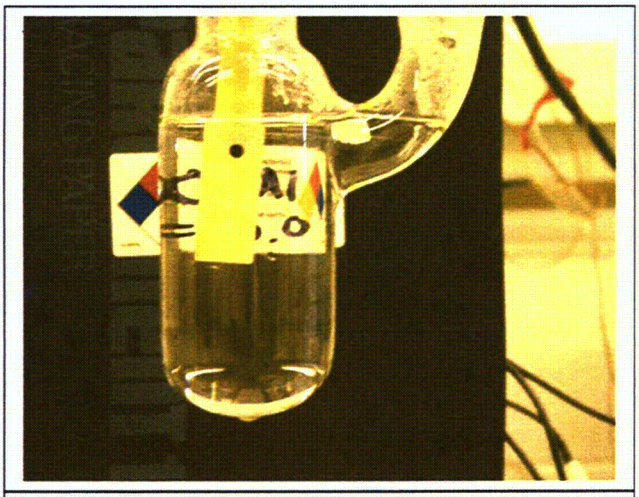

Figure D15

T= 96.3°C
t = 53 min after mixing 123.0 grams of pH =10.0 solution with 0.60 gram of $Al(NO_3)_3 \times 9H_2O$.

σ = 369 μ-MHO

Note: Oil bath removed.

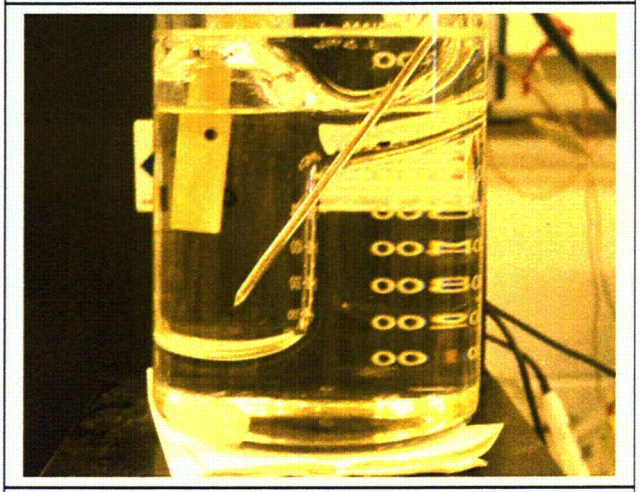

Figure D16

T= 90.3°C
t = 61 min after mixing 123.0 grams of pH =10.0 solution with 0.60 gram of $Al(NO_3)_3 \times 9H_2O$.

σ = 357 μ-MHO

Note: Oil bath in place.

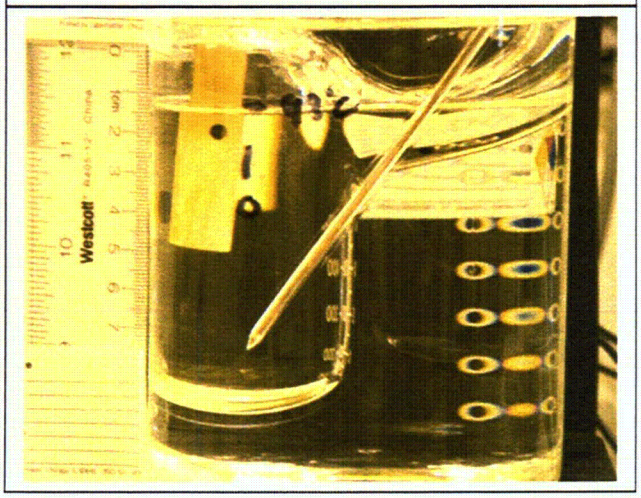

Figure D17

T= 87.0°C
t = 74 min after mixing 123.0 grams of pH =10.0 solution with 0.60 gram of $Al(NO_3)_3 \times 9H_2O$.

σ = 342 μ-MHO

Note: solution height.

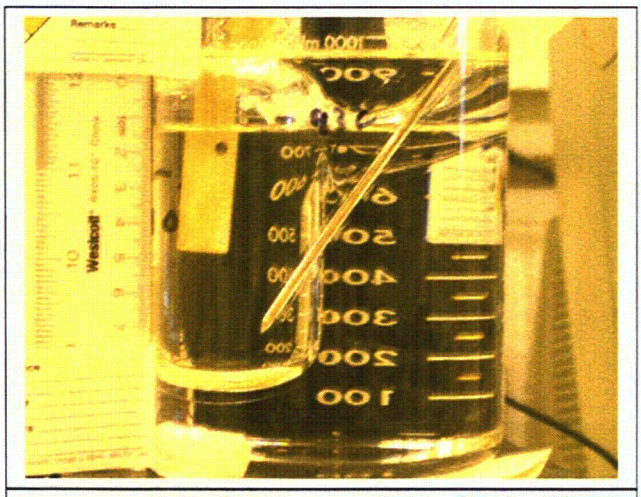

Figure D18

T= 79.0°C
t = 83 min after mixing 123.0 grams of pH =10.0 solution with 0.60 gram of $Al(NO_3)_3 \times 9H_2O$.

σ = 315 μ-MHO

Note: solution height.
Totally clear.

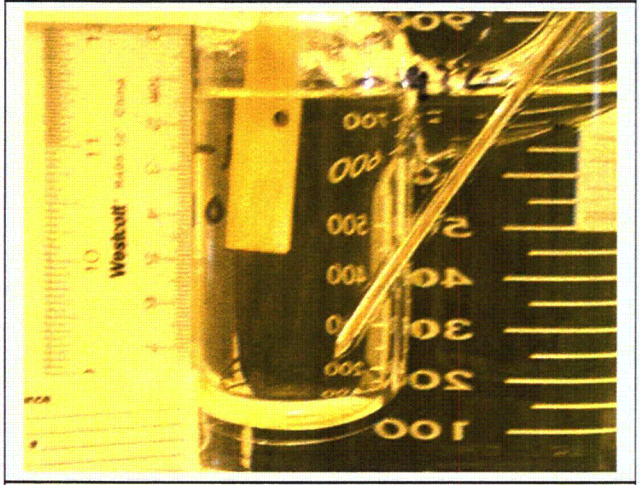

Figure D19

T= 71.2°C
t = 94 min after mixing 123.0 grams of pH =10.0 solution with 0.60 gram of $Al(NO_3)_3 \times 9H_2O$.

σ = 287 μ-MHO

Note: Totally clear

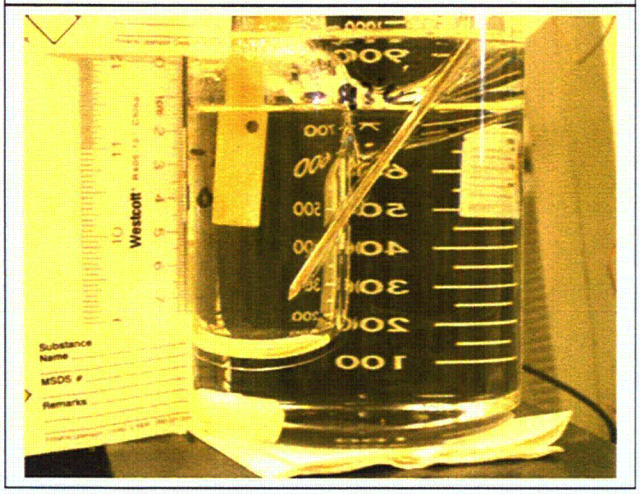

Figure D20

T= 37.0°C
t = 158 min after mixing 123.0 grams of pH =10.0 solution with 0.60 gram of $Al(NO_3)_3 \times 9H_2O$.

σ = 175 μ-MHO

Note: Totally clear

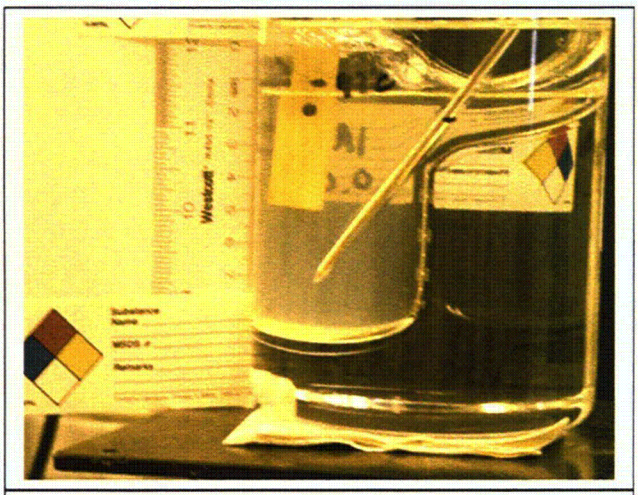

Figure D21

T= 32.0°C
t = 215 min after mixing 123.0 grams of pH =10.0 solution with 0.60 gram of $Al(NO_3)_3 \times 9H_2O$.

σ = 175 μ-MHO

Note: First time cloudiness is visible during cooling.

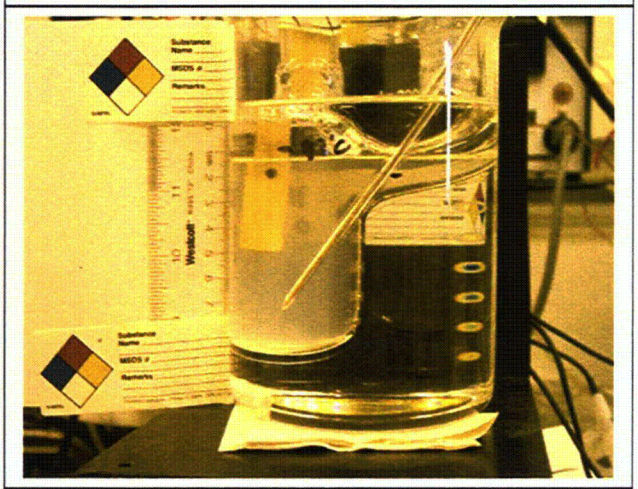

Figure D22

T= 32.0°C
t = 215 min after mixing 123.0 grams of pH =10.0 solution with 0.60 gram of $Al(NO_3)_3 \times 9H_2O$.

σ = 159 μ-MHO

Note: Cloudiness increases..

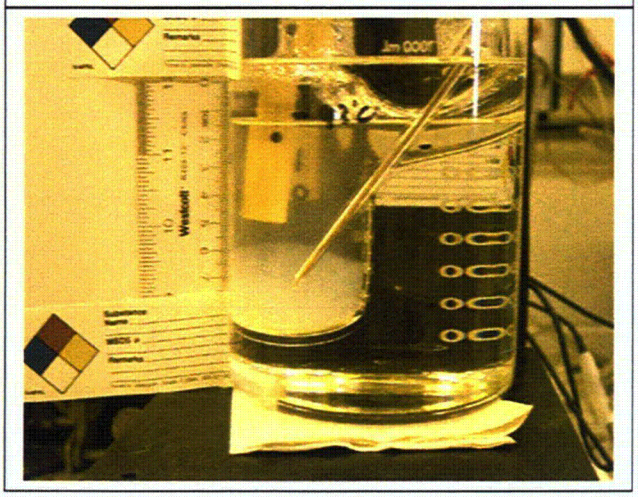

Figure D23

T= 30.0°C
t = 222 min after mixing 123.0 grams of pH =10.0 solution with 0.60 gram of $Al(NO_3)_3 \times 9H_2O$. Bottom emulsion sediments

σ = 151 μ-MHO

Note: Emulsion thickens and settles.

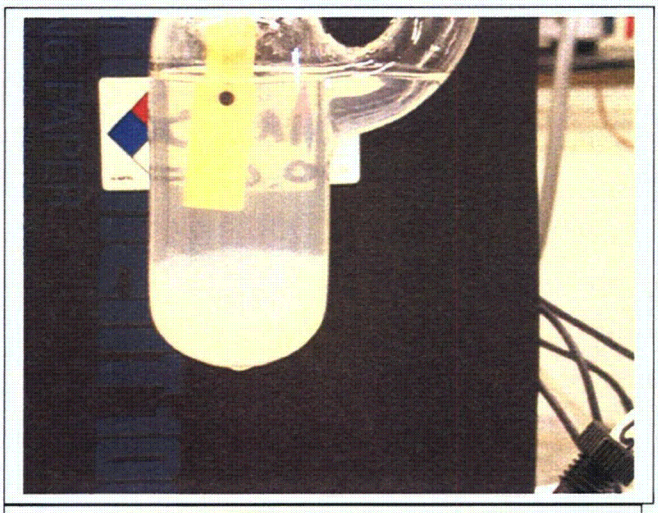

Figure D24

T= 28.0°C
t = 237 min after mixing 123.0 grams of pH =10.0 solution with 0.60 gram of $Al(NO_3)_3 \times 9H_2O$.

σ = 146 µ-MHO

Note: Oil bath removed for better view.

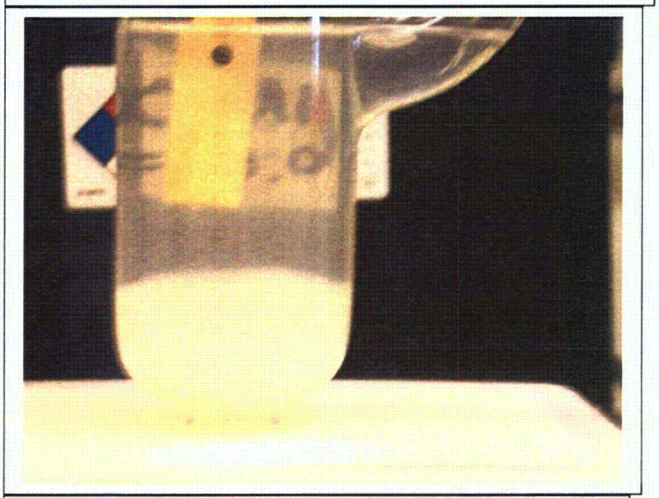

Figure D25

T= 28.0°C
t = 247 min after mixing 123.0 grams of pH =10.0 solution with 0.60 gram of $Al(NO_3)_3 \times 9H_2O$ Solution stirred by a magnetic stirrer, Oil bath out.

σ = 146 µ-MHO

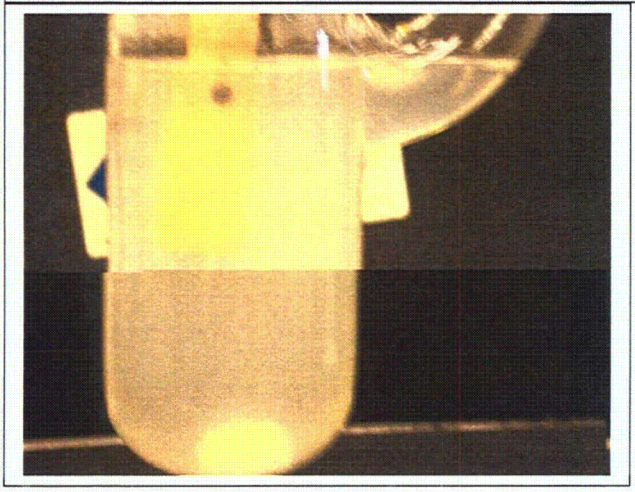

Figure D26

T= 24.6°C
t = 300 min after mixing 123.0 grams of pH =10.0 solution with 0.60 gram of $Al(NO_3)_3 \times 9H_2O$.

σ = 137 µ-MHO (without siring)
σ = 136 µ-MHO (with siring)

Note: Solution stirred with a small magnetic stirring bar (2 x 1.5 x 5 m) stirrer inside the chamber is rotating.

Appendix E NUKON dissolution Tests

Bench scale NUKON dissolution tests have been performed in four environments, ICET-1 with pH = 10 by NaOH buffering in the presence and absence of Al, ICET-3 pH = 7 with the buffering TSP, and the ICET-5 pH = 8-9 of buffering STB. The NUKON samples were exposed in the test solutions at 60°C for a test period of one month. ICP samples solution were taken at weekly intervals.

Figures E1, and E2 show SEM micrographs and EDS spectra of the NUKON before exposure. Typical fiber lengths and thicknesses were of the order of 5-mm in length and somewhat less than 10 μm in thickness. The major elements in NUKON are Si and Na, but appreciable amounts of Ca, Al, and Mg are present as shown in the EDS analysis in Fig. E2.

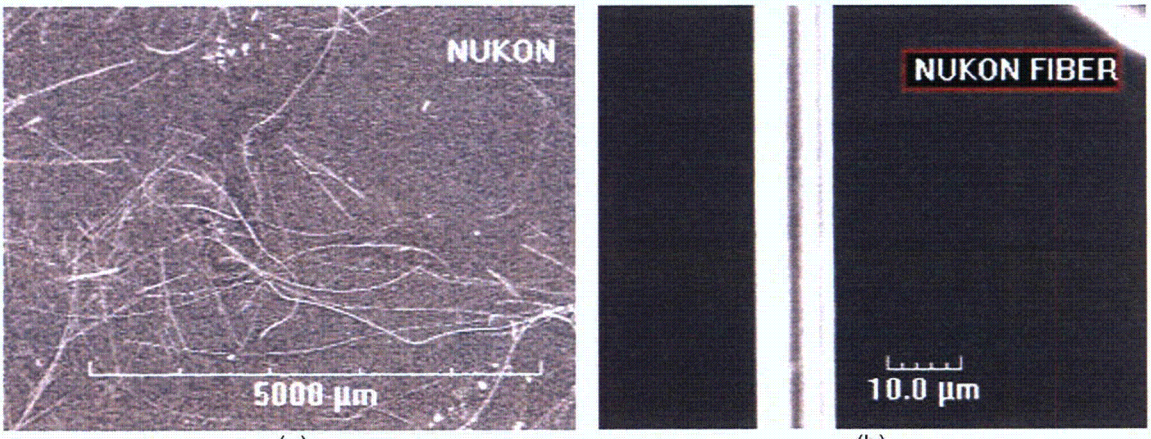

(a) (b)

Figure E1. SEM view for the NUKON Fiber (a) normal length ~0.5 mm and fiber (b) normal thickness ~10 μm

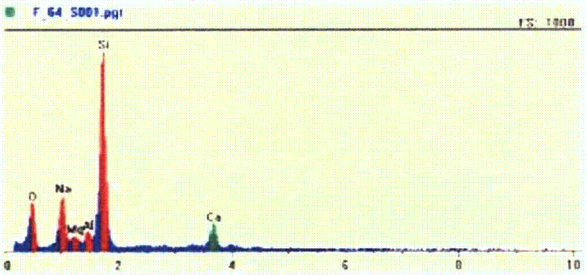

Element	KRatio	Wt%	At%
O	0.1108	32.01	44.83
Na	0.0755	13.43	13.08
Mg	0.0110	1.84	1.69
Al	0.0174	2.53	2.10
Si	0.3279	42.81	34.16
Ca	0.0627	7.39	4.13

Figure E2. EDS spectrum and elemental analysis for the NUKON Fiber

The NUKON dissolution tests were done at 60°C for a month period with a loading of 2-g NUKON/l. Table-E1 shows the matrix of the bench scale NUKON dissolution tests. The solutions were stirred with a magnetic stirrer. Samples of the supernate solution were taken each week for the ICP-analysis.

Table E1. Bench scale tests for the NUKON dissolution insulation test.

ICET	T(C)	Buffering Agent	pH	Boron (mg/l)	Note
1	60	NaOH	10	2800	NaOH concentration as required by pH.
1	60	NaOH	10	2800	NaOH concentration as required by pH. A small piece of Al metal mounted in epoxy was immersed in the solution
2	60	TSP ($Na_3PO_4.12H_2O$)	7	2800	Trisodium Phosphate concentration as required by pH.
5	60	STB (Sodium Tetraborate $Na_2B_4O_7.10H_2O$)	8 to 8.5	2400	The sodium tetraborate (STB) level was chosen to match the ICET–5 procedure. A solution with 2800 ppm B from boric acid and a solution with 2100 ppm B from STB, were mixed together to get a final solution with 2400 ppm B.

Table E2 summarizes the observations made during the dissolution tests. Figure E3 shows the three test chambers; TSP (left), NaOH (middle), and STB (right) at 60°C. Immediately after the NUKON was inserted, it sank, but in the NaOH, TSP, and STB solutions, bubbles form on the fibers and as shown in Figure E4, the NUKON floats. After a 48–h exposure, the size of the bubbles was largest in the NaOH solution, then the TSP solution, and smallest in the STB solution. In the test with Al and NaOH, the NUKON did not float during the entire test period. Figure E5 shows the NaOH, TSP, and STB exposed NUKON at the 6-days (144-h), and the Al/NaOH exposed NUKON at 73.5-h. Figure E6 shows the NaOH, TSP, and STB exposed NUKON at 7-days, and the Al/NaOH exposed NUKON at 4-days.

In the test with metallic Al, the Al mounted in the epoxy with an exposed specific surface area of 57.5 mm^2/l. Tiny bubbles could be seen forming and eventually collected as single, large bubble. Figure E7a shows a NUKON sample taken from the NaOH/Al solution at t = 118-h to investigate a black precipitate particle. A higher magnification view of the precipitate particle is shown in Fig. E7b. An EDS analysis and elemental EDS data for the black precipitate are shown in Fig. E7c. The particle is rich in Al, Na, and Si. An SEM micrograph of the Al sample after 118-h of exposure is shown in Fig. 8a, and a higher magnification view of the surface is shown in Fig. 8b.

EDS spectra with different e-beam energies were used to investigate the variation of the chemical composition with depth. The results are shown in Fig. 8c. The lower energy 4–keV beam has the lowest Si, the highest Na, and the lowest Al. This may be most representative of the chemical composition on the surface. For 7 and 10-keV beams, the Na is low which indicates that the Na stays in the surface rather penetrated into the material. The Si is higher for the high energy beams than for the 4-keV beam indicating that the Si penetrated some distance into the material. The Al compositions for the 7 & and 10-keV beams are higher than for the 4-keV beam suggesting that the corrosion product on the Al is rather thin.

ICP results for the composition of the solutions are shown in Fig. E9 and Table E3. The Si levels are noticeably lower in the solution with the Al sample. The presence of this much Al (about 1/4 the area of Al/volume as in ICET–1) clearly inhibits dissolution of the NUKON, and is consistent with the observation that this is the only NUKON with no tendency to float. The Ca is lower the solution with the

Al also, reflecting the lower dissolution rate of the NUKON. The Ca level is low in the TSP solution also, but in this case the Ca has been removed from the solution by the formation of calcium phosphate.

After about 21 days of testing, the NUKON in the STB solution disintegrated from a loose, but well–defined clump into a collection of loose fibers. The NUKON in the other solutions remained in a clump for the duration of the test. The results in Fig. E9 and Table E3 do not suggest that the dissolution rate of the NUKON in the STB solution was markedly higher than in the NaOH or TSP solutions.

Table E2. Observations of the bench scale NUKON 4 week dissolution tests at T = 60°C.

Date/time	Day of exposure	Buffering Agent			Day of exposure	Buffering Agent
	I, III, V	NaOH I	TSP III	STB V	I, Al	Al/NaOH I, Al
3-14-06 11:40am	0 (Fig. E3)	R-0 NUKON exposed	Y-0 NUKON exposed	B-0 NUKON exposed		
12:40 pm		Float: small bubbles stick with fiber. Remove bubbles let sink by glass bar	Float: small bubbles stick with fiber. Remove bubbles let sink by glass bar	Float: small bubbles stick with fiber. Remove bubbles let sink by glass bar	Started two days later]	
3-15-06 8:00 am	1	Vertical array again bubbles stick.	Vertical array again bubbles stick.			
9:00 am	1	*Remove bubbles let sink by glass bar Settled	*remove bubbles let sink by glass bar Settled	*Settled		
9:10am	1	pH = 10.11	pH = 7.13	pH = 8.88		
3-16-06 14:10am	2 (Fig. E4)				0	Start I, Al (Fig. E4)
3-17-06 10:10am	3	**Vertical array again big bobbles stick.	**Vertical array again bobbles stick.	**Vertical array again bobbles stick.	1	*NUKON settled no bubbles
3-17-06 ١٢:٣٠						
					2	
13:50		Ibid pH = 10.09	Ibid pH = 7.18	Ibid pH = 8.84-8.88	(Fig. E5)	Ibid pH = 10.10
3-20-06 11:40	6	NUKON float	NUKON ½ & ½ Sediment/float	NUKON float	4	* NUKON settled no bubbles
		(Fig. E5)				
3-21-06 8:15am	7	NUKON float R-1 pH = 10.18	NUKON ½ & ½ Sediment/float Y-1 pH= 7.45	NUKON float B-1 pH = 8.98	5	NUKON settled. Black particles on the NUKON RAl-1 pH = 10.17

Date/time	Day of exposure	Buffering Agent			Day of exposure	Buffering Agent
	I, III, V	NaOH I	TSP III	STB V	I, Al	Al/NaOH I, Al
14:00pm		Enforced bubbles detachment for settlement of NUKON	Enforced bubbles detachment for settlement of NUKON	Enforced bubbles detachment for settlement of NUKON		NUKON settled.
14:40pm		NUKON in the all three solutions stays settle down.				
3-22-06 8:15am	8	NUKON settle down. Looked relevant reaction ended (?)	NUKON settle down. Looked relevant reaction ended (?)	NUKON settle down. Looked relevant reaction ended (?)	6	NUKON settle down. Looked relevant reaction ended (?) Black particle EDS analysis see (Fig. E7,E8)
3-23-06 17:15	9	NUKON settle down, but few 2-2.5 mm dia bubbles holding with Nukon Shaken remove bubbles!	NUKON settle down. Most gentle among three, but few 2-2.5 mm dia bubbles holding with NUKON Shaken remove bubbles!	NUKON ½ floating (F) settled (S) Pushed but keeps the same ½ & ½ F/S	7	Few very small bubbles holding with Nukon Shaken remove bubbles!
3-24-06 8:15 am *Fig-9	10	Few big bubbles hold NUKON settled	Most gently settle down couple bubbles shown	ibid	8	Couple of bubbles
		(Fig. E9)				
3-26-06 8:40am	12	Yellowish High NUKON puffy	Pale disappeared Yellowish	95% NUKON float	10	Yellowish high
3-26-06 8:40am		Yellowish High NUKON puffy pH = 10.16	Pale disappeared Yellowish pH = 8.96	95% NUKON float pH = 7.35		NUKON settle down Yellowish high pH = 10.12
3-30-06 8:40am	16	R-2	Y-2	B-2	14	RAl-2
		Yellowish High NUKON puffy	NUKON settled down ; pale	NUKON float but coagulated not puffy		Same as beginning
3-31-06 8:40am	17	Ibid Nukon sink	Ibid Nukon sink	Ibid more top part of solution	15	Ibid Nukon sink

Date/time	Day of exposure	Buffering Agent			Day of exposure	Buffering Agent
	I, III, V	NaOH I	TSP III	STB V	I, Al	Al/NaOH I, Al
4-4-06	21	R-3	Y-3	B-3	18	RAl-3
8:40am		NUKON down less puffy pH = 10.19	NUKON down pale Puffy pH = 7.53	*70% NUKON powdered except 30% coagulations in float Solution very fuzzy pH = 9.00		NUKON down same More black ppt on the NUKON pH = 10.11
4-11.04 14:26 pm	28	R4	Y-4	B-4	25	RAl-4

Note: ICP-sample code as, R-#, RAl-#, Y-#, B-#, # = 0, t = 0, and # = 0, 1, 2, 3, 4. Where R = NaOH solution, RAl = Al/NaOH, Y = TSP solution, and B = STB solution respectively. # stand for the week, e.g., R-1 = NUKON dissolution period one week in NaOH solution.

Figure E3.
NUKON (2-g/l ratio) exposed in three different solutions; TSP (left), NaOH (middle), and STB (right) at 60°C.

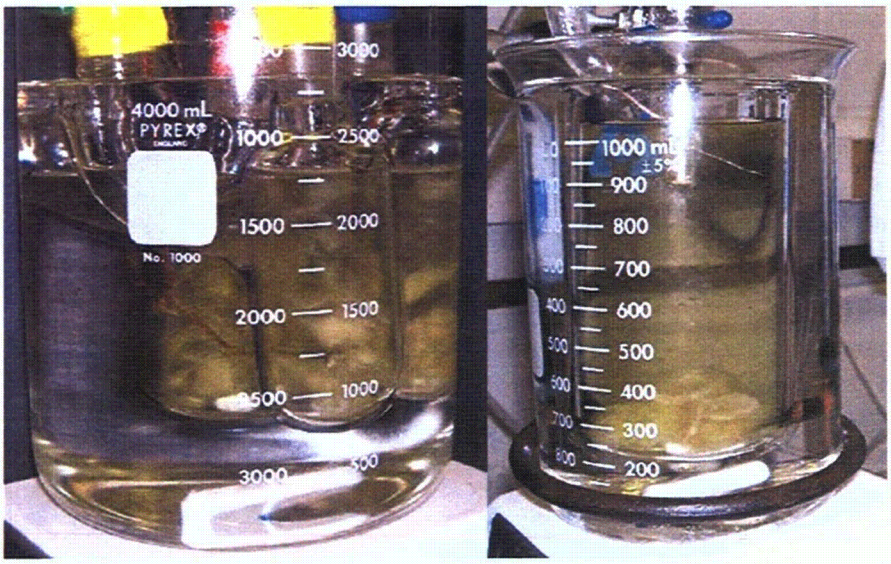

Figure E4. On the left are the tests in NaOH, TSP, and STB solutions at 48–h. The NUKON floats due to the bubbles becomes stick on the fiber surface. On the right side is the Al/NaOH test. The NUKON remained at the bottom of the chamber through the whole test period.

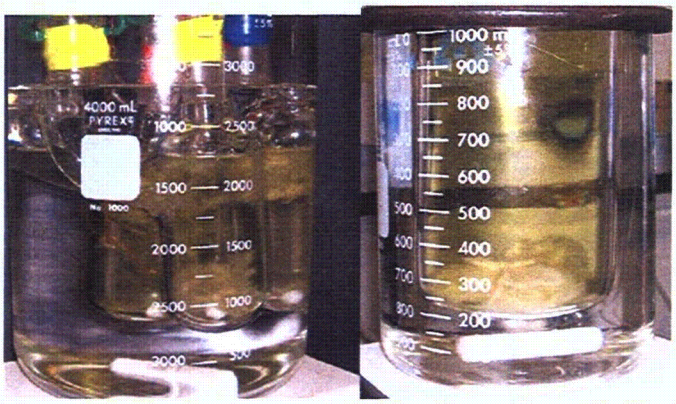

Figure E5.
The NUKON floating due to the bubbles on the fiber surface at 144–h. NUKON in NaOH (red) and STB (blue) totally floating, and TSP ½ & ½ float/sediment (Yellow). In the Al/NaOH solution at 73.5–h on the right, the NUKON remains settled .

Figure E6. The NUKON enforced settled 40-min ago for popping up the bubbles by glass rod to learn the bubble formation profile in this period of exposure. Time = 167.58-h, T = 60°C. For the Al/NaOH, NUKON settled down from the beginning. Time = 97.08-h, T = 60°C

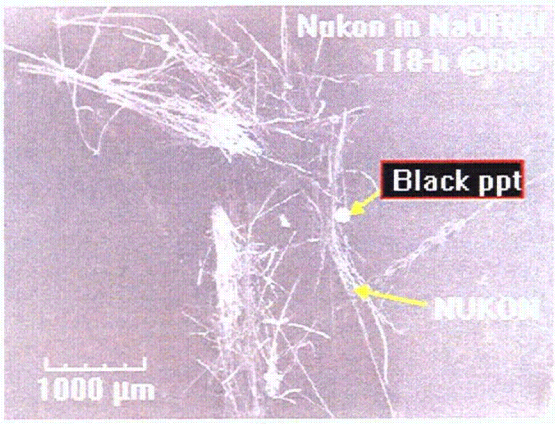

(a)

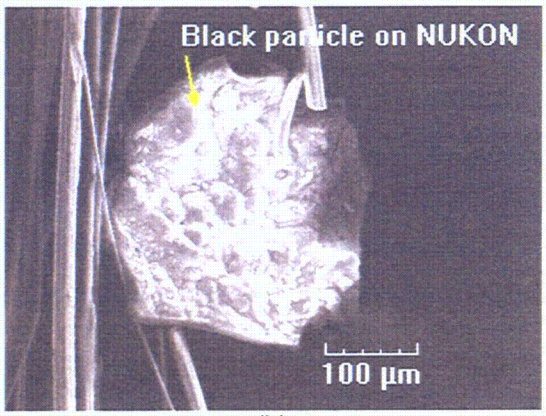

(b)

Element	Wt%	At%
Na	**15.17**	**17.72**
Mg	5.71	6.31
Si	**27.72**	**26.51**
Ca	2.14	1.44
Fe	1.98	0.95
Al	**47.27**	**47.07**

(c)

Figure E7.
(a) Sample of NUKON from the dissolution test in NaOH/Al pH = 10 at 60°C (t = 118-h) with a black-precipitate particle; (b) higher magnification of the particle ; (c) EDS spectra and EDS data for the black precipitate.

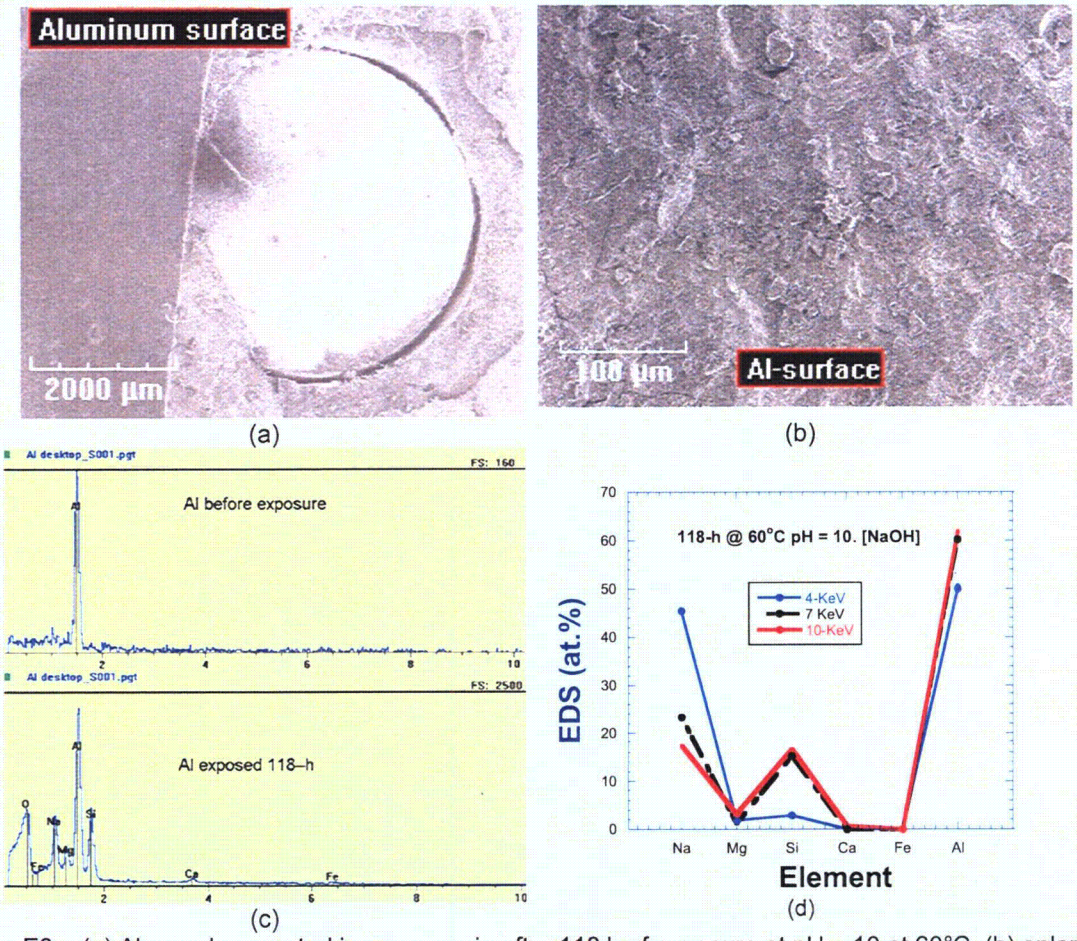

Figure E8. (a) Al sample mounted in epoxy resin after 118 h of exposure at pH = 10 at 60°C, (b) enlarged SEM micrograph for the corroded Al surface, and (c) EDS spectra of the surface of the Al before exposures and after 118–h exposure and (d) composition of elements from EDS spectra with different e-beam energy to assess the variation of the chemical composition with depth.

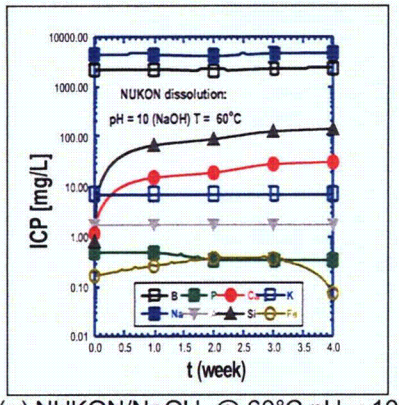

(a) NUKON/NaOH @ 60°C pH = 10

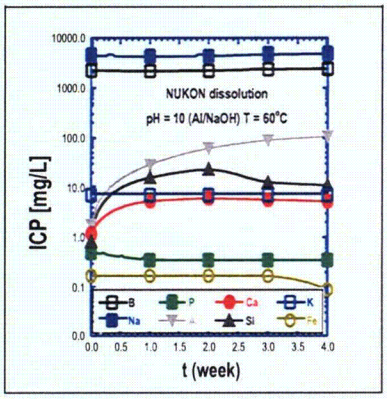

(b) NUKON/Al: NaOH @ 60°C pH = 10

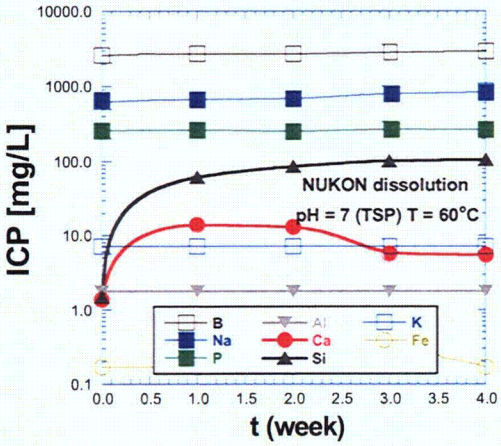

(c) NUKON/TSP @ 60°C pH = 7-7.3

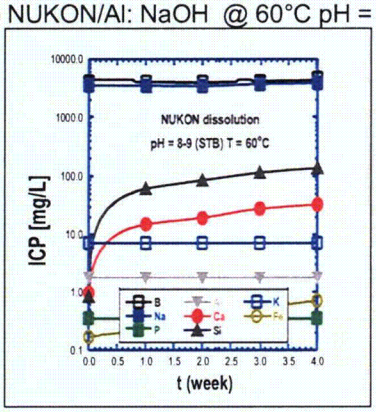

(d) NUKON/STB @ 60°C pH = 8-9

Figure E9. Elemental ICP for the bench NUKON dissolution testes in ICET-1 (a) NaOH, (b) NaOH/Al, (c) ICET-3 (TSP), and (d) ICET-5 (STB) with the loading 2-g NUKON/l at 60°C in the ambient condition for a period of 4 weeks.

Table E3. Elemental ICP for the bench scale 4-week NUKON dissolution tests

Sample	time	Elements ICP (mg/l)								
	wk	Al	B	Ca	Fe	K	Mg	Na	P	Si
NaOH	0	<1.79	2,270	1.16	0.17	7.07	1.90	4,460.70	0.50	0.84
ICET-1	1		2,270	15.50	0.27	7.07	2.52	4,362.50	0.49	70.55
	2		2,140	19.20	0.38	7.07	2.18	4,121.30	0.35	92.78
	3		2,360	28.80	0.37	7.07	2.36	4,661.40	0.35	132.61
	4		2,400	31.53	0.08	7.07	1.90	4,788.00	0.35	147.67
TSP	0	<1.79	2,610	1.38	0.17	7.07	1.90	619.21	257.25	1.51
ICET-3	1		2,740	14.02	0.17	7.07	5.64	667.10	262.98	61.81
	2		2,720	13.11	0.17	7.07	7.25	683.81	251.66	86.51
	3		2,850	5.71	0.25	7.07	8.29	794.48	267.95	102.82
	4		2,950	5.45	0.17	7.07	4.21	830.55	266.62	106.29
STB	0	<1.79	2,270	0.96	0.17	7.07	1.90	3,567.30	0.35	0.84
ICET-5	1		2,610	15.15	0.22	7.07	5.32	3,518.50	0.35	61.72
	2		2,270	19.44	0.24	7.07	6.31	3,453.90	0.35	85.29
	3		2,360	28.10	0.51	7.07	9.39	3,732.90	0.35	115.32
	4		2,390	33.33	0.71	7.07	11.19	3,893.70	0.35	138.37
Al/	0	<1.79	2,270	1.16	0.17	7.07	1.90	4,460.70	0.50	0.84
NaOH	1	29.21	2,200	5.27	0.17	7.07	1.90	4,206.80	0.35	16.16
ICET-1	2	61.89	2,240	6.01	0.17	7.07	1.90	4,324.90	0.35	23.77
	3	90.80	2,390	5.65	0.17	7.07	1.90	4,650.30	0.35	12.81
	4	107.48	2,450	5.20	0.09	7.07	1.90	4,780.20	0.35	11.28

A replicate test on NUKON dissolution in the various test environments was performed. In most respects the behavior was similar in the two tests. However, in this case, in the STB solution only a small portion of the NUKON was dispersed. In the NaOH/Al solution a portion of the NUKON did begin to float during the test.

Appendix F: Test plan for comparison benchmark testing of PNNL and ANL test loops

C. W. Enderlin and B. E. Wells, Pacific Northwest National Laboratory

F1 Objective

The objective of the tests is to benchmark the test loops at PNNL and ANL against each other by comparing head loss measurements as a function of screen approach velocity, debris bed dimensions, and post-test debris mass measurements. These benchmark tests will allow for the comparison of the debris injection processes and measurement systems for the two loops. The debris material preparation and the debris bed formation process will be duplicated, as much as possible, to accomplish this.

F2 Background

The following items are issues that have been considered in selecting the benchmark test cases and for determining the test conditions that need to be defined in an attempt to ensure the initial conditions are the same in each test loop:

- Both the ANL and PNNL test loops have 6-in. diameter test sections.
- The maximum head loss across the debris bed that can be measured is 165 and 2700 inches H_2O for the ANL and PNNL loops, respectively.
- The method of introducing the debris material into the test loop is different for each test loop.
- Testing conducted by PNNL has demonstrated that the degree of debris preparation for the Nukon debris material impacts the head loss of a debris bed. A metric (referred to as R4, see Section 4.1.1) and associated method of evaluation have been developed for assessing the degree of Nukon preparation.
- For debris beds containing both CalSil and Nukon, preliminary testing conducted to date by PNNL indicates that the loading sequence of the debris constituents can have a significant impact on the measured head loss for the resulting debris bed.[1]
- PNNL test results conducted in the bench top loop indicated that repeatable results were obtained for CalSil-Nukon debris beds having a CalSil to Nukon mass ratio of approximately 0.2. Significant variations in measured head loss, in both the large-scale and bench top loops, were obtained for debris beds having a CalSil to Nukon mass ratio of 0.5. The variation in the results for the higher mass ratios is still being investigated.
- Test 050803_NO_0682_2 conducted in the PNNL bench top loop consisted of a Nukon debris bed with a target mass loading of 0.035 lbm/ft^2 (0.841 kg/m^2) and an R4 of approximately 11. Head loss measurements of approximately 14 and 124 inches H_2O were obtained for screen approach velocities of 0.16 and 0.65 ft/s respectively.
- Test 051004_NC_1469_1 conducted in the PNNL bench top loop consisted of a Nukon and CalSil debris bed with a total target mass loading of 0.076 lbm/ft^2 (1.812 kg/m^2). The Nukon target mass loading was 0.061 lbm/ft^2 (1.449 kg/m^2) with an R4 of approximately 11. The CalSil target mass loading was 0.015 lbm/ft^2 (0.363 kg/m^2), for a CalSil to Nukon mass ratio of 0.25. Head loss measurements of approximately 280 and 504 inches H_2O were obtained for screen approach velocities of 0.15 ft/s and 0.25 ft/s respectively.

[1] *Investigation of the Effect of Loading Sequences for Significant Head Loss Differences from Similar Nukon/CalSil Debris Beds*, 1/16/05, CW Enderlin and BE Wells to WJ Krotiuk.

- ANL testing indicates the resulting head loss measurements have been more stable when the screen approach velocity is decreased following debris bed formation as opposed to increasing the approach velocity following bed formation. When the approach velocity is decreased from that initially used to generate a debris bed, ANL has obtained steady state pressure drops very quickly compared to the time duration required when the velocity is increased.
- The bulk of ANL testing has been conducted taking head loss measurements for approach velocities in the range of 0.02 to 0.1 ft/s. The bulk of the ANL debris beds have bed formed at an approach velocity of 0.1 ft/s followed by incrementally ramping down the approach velocity.
- The PNNL testing has been conducted taking head loss measurements over the range of approximately 0.02 to 1.0. ft/s with the bulk of the measurements taken between 0.1 to 0.4 ft/s. Debris beds have been generated in the PNNL large scale test loop at approach velocities of 0.1 and 0.2 ft/s followed by incrementally ramping up the approach velocity.
- PNNL has formed the debris beds with the fluid temperature at approximately 20°C (68°F). The PNNL loop in its current configuration is designed to introduce the debris material at a fluid temperature ≤ 40°C (104°F).

F3 Test Matrix

The test cases were selected from the proposed test matrix, dated 12/1/05, WJ Krotiuk prepared for the Series II tests to be conducted at PNNL. The test cases were selected based on the following objectives/criteria.

- Test two Nukon-only cases and one Nukon/CalSil case.
- The Nukon cases should consist of a relatively thin bed (app 0.04 lb/ft^2 [0.2 kg/m^2]) and a relatively medium bed (app 0.16 lb/ft^2 [0.8 kg/m^2]).
- The Nukon/CalSil case will use the same Nukon mass loading as one of the two Nukon-only cases to reduce variations in debris preparation process between debris beds.
- The CalSil/Nukon ratio should be ≤ 0.25.
- Only cases that have an anticipated head loss ≤ 160 inches H_2O at an approach velocity of 0.2 ft/s should be selected to ensure head loss data can be obtained over a one order of magnitude range of approach velocities in both test loops.

Based on the background information presented in Section 2.0 and the previously defined selection criteria, the three cases presented in Table 1 have been selected for the benchmark tests. Each test case will be conducted once and results submitted to the NRC for evaluation and direction on performing repeat tests for selected test cases.

Table F1. Benchmark test cases for ANL and PNNL test loops

Case No.	Nukon Mass Loading lb/ft^2 (kg/m^2)	CalSil Mass Loading lb/ft^2 (kg/m^2)	Total Mass Loading lb/ft^2 (kg/m^2)	CalSil to Nukon Mass Ratio
BM-1	0.044 (0.217)	0.0 (0.0)	0.044 (0.217)	0.0
BM-2	0.148 (0.724)	0.0 (0.0)	0.148 (0.724)	0.0
BM-3	0.148 (0.724)	0.030 (0.145)	0.178 (0.869)	0.2

F4 Test Preparation

The test preparation is specified in an attempt to control the initial conditions at which the debris bed is formed on the screen. Test preparation consists of the test loop conditions, the preparation of the debris material, and the conditions at which the debris bed is formed. The system and method by which the debris material is physically introduced into the test loop will not be specified and is part of the conditions being qualified by these benchmark tests. Section 4.1 summarizes how the debris material will be prepared prior to introduction. The test loop conditions at the start of testing are discussed in Section 4.2, and the parameters specifications for bed formation are presented in Section 4.3.

F4.1 Debris Preparation

The CalSil and Nukon debris material to be used for the tests will be from the following sources:

- The Nukon material will come from Vendor/Manufacturer: Performance Contracting Inc., Lot No.: 09/06/5ND5, BS-4813 shipped: Oct. 8, 2005. This material was subjected to a 12 to 24 hr heat-treating process and shredded by the vendor/manufacturer prior to shipment.
- The CalSil material will come from Vendor/Manufacturer: Johns Manville, Lot No.: 017-276, BS-4823, shipped: September 28, 2005. The received CalSil material will be in the form of 3-in. by 12-in. by 48-in blocks. The CalSil material has not been subjected to any heat-treating process.

The preparation of the Nukon and CalSil materials is discussed in Sections 4.1.1 and 4.1.2, respectively

F4.1.1 Nukon Preparation

The debris preparation method for the Nukon used in the benchmark tests will be characterized by the R4 metric and the debris dilution used for blending. The R4 metric is defined by

$$R4 = \frac{\text{Nukon and Water Mass on Screen}}{\text{Initial Nukon Mass}} \qquad (1)$$

The as-received "shredded" Nukon will be added to a specified volume of water and blended using an industrial bench top blender to separate/breakdown (i.e. "reduce") the fibrous material. The degree of blending and the amount of dilution for each test case will be obtained from trying to replicate the degree of material "reduction" performed by ANL for their most recent tests.

During past work at LANL the shredded Nukon fiber was boiled for duration of 10 to 15 minutes prior to being introduced to the loop. The boiling was performed to break down organic binders. ANL currently subjects the debris material to a "pre-soak," which consists of soaking the material in 140°F water for 30 minutes prior to introduction into the loop. The 30-min. pre-soak is intended to simulate the approx. 30 min. delay that would exist between the occurrence of a LOCA and the start of the circulation pump. To eliminate a potential source of variability, no "pre-soak" or boiling of the Nukon will be performed for the benchmark tests.

To determine the R4 metric, ANL will carry out their Nukon preparation method a minimum of three times for each of the Nukon mass loadings specified in Table 1. The preparation method will use a constant Nukon mass and water volume for each batch and sub-batch of material generated.

Definition: Debris batch – The entire mass of a debris constituent that needs to be prepared to conduct a specific test. Example: Test case BM-2 requires 13.22 g of Nukon be introduced to the loop, therefore, the "batch" of Nukon for a test run for Case BM-2 is 13.22 g.

Definition: Debris sub-batch – The amount of mass that is to be placed in a single mixer for blending that is to be combined with other sub-batches to generate a single debris batch for testing. If the entire mass of a debris batch can be prepared in a single operation of the blender then no debris sub-batches are necessary.

The generation of a debris batch using sub-batches should attempt to use uniform sub-batches. Example: Suppose the required debris batch has a mass of 45 g, and the blender to be used can hold 500 ml of water and concentrations up to 30 g Nukon in 500 ml water can successfully be blended. A blend time and dilution rate should be determined for preparing three debris sub-batches of 15 g each. It would not be desirable to prepare two sub-batches of 20 g each using a specified dilution rate and blend time and then prepare a third sub-batch of 5 g using a second dilution rate and blend time.

Based on previous work conducted by LANL, the maximum concentration to be used for blending sub-batches of Nukon is 25g Nukon per1000 ml water.

After ANL prepares each debris sub-batch intended for the purpose of determining R4, an R4 test will immediately be conducted to determine the wet mass of material retained on the screen. The mass of Nukon retained on the screen will be photographed after each R4 test. The R4 tests will be conducted using 5-mesh screen. For each quantity of Nukon specified in Table 1, the following information will be transmitted to PNNL:

- Individual R4 values calculated by ANL
- Dimensions of the 5-mesh screen used to conduct the R4 test,
- The volume or mass of water used to generate a debris batch/sub-batch,
- The mass of dry Nukon used to generate a debris batch/sub-batch,
- Blender make and model number,
- Photographs of the retained mass on the screen taken following each R4 test.

Note 4.1.1 - A: The debris material used to conduct an R4 test will never be introduced to the test loop. Once the dilution ratio and blend times have been determined and assessed via multiple R4 tests, the debris preparation procedure is executed to generate a debris batch for introduction into the loop. This prepared debris batch does not undergo an R4 test.

Note 4.1.1 – B: The retained mass on a screen following an R4 test is to be removed prior to executing a new R4 test.

PNNL will attempt to use the same dilution ratios as ANL and determine blending times required to achieve an average R4 value of within ± 1 of the average ANL value for each quantity of Nukon required for the debris loadings specified in Table 1. Conducting R4 tests on a minimum of three debris batch preparations will assess the final R4 value for the PNNL tests.

F4.1.2 CalSil Preparation

The CalSil will be prepared by mortar and pestle on the dry debris material. The CalSil will be ground until no visible large particles exist. The final product should have the CalSil material disassociated from the fibrous component and the ground material should have the consistency of flour. Based on past observations by LANL it is recommended that relatively small sub-batches of CalSil should be ground separately to achieve the desired consistency. LANL observed that the separated fiber might tend to aggregate during continued grinding.

The dry ground material (including both the fiber and particulate) will then be added to water and blended in the blender. The dilution ratio of the dry CalSil and the blending time will be the same as that currently employed by ANL.

No "presoak" or boiling of the CalSil will be performed for the benchmark tests.

ANL will provide PNNL with the following:

- Photographs of the dry CalSil material following grinding using mortar and pestle.
- The dilution ratio of CalSil to water used for blending operations.
- The blending time used for a CalSil debris batch/sub-batch.
- Blender make and model number.
- A physical description of the appearance and pour ability of the CalSil slurry following blender operations.
- Photographs of the CalSil slurry.

PNNL will perform PSDA on a CalSil slurry prepared according to the final CalSil preparation procedure used for the benchmark tests.

F4.1.3 Debris Preparation for Introduction to Loop

Following the preparation of the concentrated debris slurries discussed in Sections 4.1.1 and 4.1.2, there are three imposed debris preparation requirements for introduction of the debris material into the loop. This portion of the process is unique to the individual test loops and is being assessed by these benchmark tests. The three requirements are:

- The CalSil and Nukon materials are to be pre-mixed by manual stirring with a kitchen utensil prior to introduction into the test loop.
- The concentrated CalSil and Nukon slurries are to be prepared just prior to testing.
- The prepared, mixed slurry is to continually experience some form of mild agitation to prevent material settling and agglomeration prior to introduction into the test loop. Past experience has demonstrated that manual stirring with a kitchen utensil is sufficient.

F4.2 Test Loop Conditions

The test loops will use perforated plate as the sump pump screen aligned in a horizontal orientation perpendicular to the flow in a vertical test section. The perforated plate will have the dimensions specified in Table 2. Due to the manufacturing process, the holes in the perforated plate will have a

squared edge and a rounded edge. The plate is to be installed with the rounded edges of the holes directed upstream.

Table 2. Perforated Plate Dimensions

Diameter of Perforations (in.)	Center to Center Pitch (in.)	Hole Pattern	Percent Open Area (%)	Plate Thickness (in.)
1/8	3/16	Staggered 60° centerline pattern	40	0.056

The test loop is to be flushed and inspected (based on past practices and assessments made for the individual loops) to ensure minimal residual free debris material exists from past testing.

The loop is to be filled with DI water for testing. Degassing of the water should be conducted to minimize/eliminate the presence of gas in the system during testing.

F4.3 Debris Bed Formation

The diluted, premixed debris slurry is to be continually agitated prior to introduction into the loop as specified in Section 4.1.3. The debris slurry is to be introduced into the test loop with the screen approach velocity adjusted to 0.1 ft/s. The approach velocity is defined as the average velocity in the upstream test section. The retention of debris material on the test screen will cause a change in the system curve for the test loop resulting in an increase in pressure drop across the debris bed and a corresponding reduction in screen approach velocity. During debris bed formation the screen approach velocity is to be maintained between 0.09 and 0.1 ft/s.

The fluid temperature during bed formation and for the duration of the test is to be maintained at 25° ± 5°C (77° ± 9°F).

The indicated head loss is to be sampled at a minimum frequency of 0.5 Hz and monitored with a running 1-minute average of the sampled data. The head loss data is to be logged at a minimum frequency of 0.1 Hz. The debris bed formation process will be considered complete when both of the following two criteria have been satisfied.

1. A minimum time equivalent to 20 calculated loop circulations assuming a constant screen approach velocity of 0.1 ft/s has elapsed.
2. The absolute change in head loss based on a 1-minute running average is less than 2% over 10 minutes. The criteria will be assessed and satisfied three times. The minimum time between assessments will be one minute. The criteria is expressed as

$$0.02 \geq \left| \frac{\Delta P_{t_1} - \Delta P_{t_2}}{\Delta P_{t_1}} \right|$$

Where: ΔP_{t1} = the measured head loss across the bed at time t_1.
ΔP_{t2} = the measured head loss across the bed at time t_2.
$t_1 - t_2 \geq 10$ minutes

Exception: For head loss measurements less than 14 inches H_2O (0.5 psi) the acceptance criteria will be:

$$0.05 \geq \left| \frac{\Delta P_{t_1} - \Delta P_{t_2}}{\Delta P_{t_1}} \right|$$

At the completion of bed formation the following will be recorded:

- Photographs of the debris bed
- Measurements of the debris bed thickness
- Time duration between debris introduction and steady state head loss readings.

F5 Testing & Measurements

The actual testing is considered to commence after the debris bed has been formed (data will be taken over the entire test period including static loop conditions, flow initialization, bed formation, etc.). The objective of the items discussed in Section 4.0 is to generate a debris bed in each loop for a given test case that is similar. This section defines the success criteria for the benchmark tests in Section 5.1, presents current issues associated with the test plan in Section 5.2, outlines the test process in Section 5.3, and discusses post test measurements in Section 5.4,

F5.1 Success Criteria

The success criteria for this test plan is to obtain, from both ANL and PNNL, data from one test for each test condition listed in Table I. The data is to include head loss measurements for the velocity sequence presented in Table 3. The steady state head loss measurements and post-test debris bed measurements will be used to compare the measurement and debris injection systems for both loops. Following the initial comparison of the test results, the NRC will determine if additional testing is required under this test plan.

F5.1.1 Discussion of Success Criteria

Disregarding experimental uncertainty associated with carrying out the test preparation tasks, the differences between debris beds generated in the two loops should be the result of random variation associated with the debris bed formation process and the differences in the debris injection methods. The random variation associated with debris bed formation can be investigated with repeat tests in the individual test loops. The variations due to the physical debris loading process may only be distinguishable at small velocities (≤ the bed formation velocity) and may be eliminated with exposure to higher velocities.

It is plausible that differences, which exist immediately following bed formation, between the debris beds generated in the two tests loops will be eliminated or reduced as a result of subjecting the debris bed to velocity cycling or increased pressure drop. Therefore, the two test loops may yield different measurements of head loss until a threshold pressure drop is achieved, and then display acceptable agreement. No definition has been given for acceptable benchmarking. Example: Has successful benchmarking been achieved if it requires five velocity cycles or testing at velocities greater than 0.2 ft/s to achieve good agreement between the two test loops?

No criteria have been given for the repeatability requirements of an individual test loop.

F5.1.2 Potential Success Criteria for the Benchmark Tests

- Complete one test in both the ANL and PNNL test loops for each test case (refer to Table 1).
- Obtain average steady state measurements as a function of approach velocity for the two test loops that are within 10 % of each other after two cycles of velocity ramp up and down.

F5.2 Test Plan Issues

This section presents several issues that should be considered in determining whether the current test plan is sufficient to meet the stated objectives and the project needs. The issues are also items that should be considered when comparing the measurements obtained from the two loops .

The current test plan calls for generating the debris beds at a screen approach velocity of 0.1 ft/s (0.030 m/s). During Series I testing at PNNL it appeared that debris settled within the loop during the debris formation process. This settled material appeared to be resuspended at higher velocities later during the test. If settling of debris material occurs, then the debris beds may vary in mass for the initial test measurements until material is potentially resuspended at a higher velocity and deposited on the debris bed. The material may not be resuspended since the critical velocity to sustain suspension for a given material at a specific concentration can be lower than the critical velocity for resuspension. If variations in the results are encountered between the two test loops and a discrepancy is observed in the post-test debris bed mass measurements, it is recommended that consideration be given to repeating the test case with a greater debris bed formation velocity.

The inventory of the PNNL test loop is approximately twice that of the ANL loop. The potential for this difference between the test loops to create significant differences in head loss measurements is considered minimal as long as debris material does not settle during the bed formation process. The following issues should be considered when comparing test results from the two loops.

- If material settles during bed formation, at increased velocities the addition of debris to the retained debris bed could be expected to occur at twice the rate in the ANL loop. This effect could explain the observation of results being comparable at lower velocities and then deviating at higher velocities (at least for the first velocity ramp-up at velocities greater than the bed formation velocity).
- The debris bed in the PNNL loop will be subjected to flow for a longer period of time to obtain a similar retained mass as in the ANL loop.

It is recommended by PNNL that the test program should not rely on obtaining pressure drop data for screen approach velocities in the transition flow regime.[2] The current velocity sequence presented in Section 5.3, Table 3 has head loss measurements being taken at steady state velocities predicted to create a transition flow in the test section. At a temperature of 21°C (70°F), the transition flow regime is predicted to exist for screen approach velocities from 0.009 to 0.026 m/s (0.031 to 0.085 ft/s). At a temperature of 93°C (140°F), the transition flow regime is predicted to exist for screen approach velocities from 0.005 to 0.012 m/s (0.015 to 0.041 ft/s). It is recommended that the head loss

[2] *Revised Memo on Impact of Test Section Diameter and Fluid Approach Velocity on Reynolds Number*, 5/19/05, CW Enderlin to WJ Krotiuk.

measurements be taken for the entire velocity sequence, but the potential flow regime issue should be considered when comparing test results between the two loops.

F5.3 Test Process

After the debris bed has been formed and the criteria for steady state conditions met, the bed will be subjected to a sequence of velocities that are listed in Table 3. Each approach velocity will be maintained until a steady state head loss has been achieved. A steady state head loss will be assumed after all of the following three requirements have been met:

1. The steady state velocity has been maintained for a minimum of 5 minutes.
2. If the current velocity is the peak velocity at the end of a ramp up, then the steady state velocity has been maintained for a minimum of 10 minutes.
3. The absolute change in head loss based on a 1-minute running average is less than 2% over 5 minutes. (Exception: For head loss measurements less than 14 inches H_2O (0.5 psi), the absolute change in head loss based on a 1-minute running average will be less than 5% over 5 minutes). The criteria will be assessed and satisfied three times. The minimum time between assessments will be one minute.

Table 3. Velocity sequence for the ANL and PNNL test loop benchmark cases

Test Point	Velocity (ft/s)	Test Sequence
Initial condition	0.10	Bed Formation
1	0.10	Ramp down 1
2	0.05	Ramp down 1
3	0.02	Ramp down 1
4	0.05	Ramp up 1
5	0.10	Ramp up 1
6	0.05	Ramp down 2
7	0.02	Ramp down 2
8	0.10	Ramp up 2
9	0.15	Ramp up 2
10	0.20	Ramp up 2
11	0.15	Ramp down 3
12	0.10	Ramp down 3
13	0.15	Ramp up 3
14	0.20	Ramp up 3
15	0.10	Ramp down 4
16	0.05	Ramp down 4
17	0.02	Ramp down 4
18	0.10	Ramp up 4

The fluid temperature during testing is to be maintained at 25° ± 5°C (77° ± 9°F). The velocity test matrix/sequence to be performed is presented in Table 3.

If ANL obtains head losses greater than 160 inches H_2O for any test case, a velocity, which yields a head loss between 150 to 160 inches H_2O, will be substituted, for the individual test case, for the peak velocity in Table 3. The revised velocity sequence for the specified test case will be transmitted to PNNL.
After a steady state head loss has been achieved:

- The head loss across the debris bed and fluid velocity measurements will be recorded for a minimum of two minutes at a minimum of 0.1 Hz.
- The debris bed height will be measured
- The fluid temperature in the loop will be measured.

F5.4 Post Test *Measurements*

After the velocity sequence in Table 3 has been executed the debris bed is to be retrieved for post-test analyses. Post-test measurements are to include:

- Debris bed height along two perpendicular diameters.
- The mass of the wet retrieved debris bed.
- The dry mass of the retrieved debris bed as a function of time demonstrating a constant mass has been achieved at an elevated temperature. PNNL currently dries the debris beds at 90° C and ambient pressure.

NRC FORM 335
(9-2004)
NRCMD 3.7

U. S. NUCLEAR REGULATORY COMMISSION

BIBLIOGRAPHIC DATA SHEET

(See instructions on the reverse)

1. REPORT NUMBER
(Assigned by NRC. Add Vol., Supp., Rev., and Addendum Numbers, if any.)

NUREG/CR-6913
ANL-06/41

2. TITLE AND SUBTITLE

Chemical Effects Head-Loss Research in Support of Generic Safety Issue 191

3. DATE REPORT PUBLISHED

MONTH	YEAR
December	2006

4. FIN OR GRANT NUMBER

N6100

5. AUTHOR(S)

J.H. Park, K. Kasza, B. Fisher, J. Oras, K. Natesan, and W.J. Shack

6. TYPE OF REPORT

Topical

7. PERIOD COVERED (Inclusive Dates)

8. PERFORMING ORGANIZATION – NAME AND ADDRESS *(If NRC, provide Division, Office or Region, U.S. Nuclear Regulatory Commission, and mailing address; if contractor, provide name and mailing address.)*

Argonne National Laboratory
9700 South Cass Avenue
Argonne, IL 60439

9. SPONSORING ORGANIZATION – NAME AND ADDRESS *(If NRC, type "Same as above"; if contractor, provide NRC Division, Office or Region, U.S. Nuclear Regulatory Commission, and mailing address.)*

Division of Fuel, Engineering and Radiological Research
Office of Nuclear Regulatory Research
U.S. Nuclear Regulatory Commission
Washington, DC 20555–0001

10. SUPPLEMENTARY NOTES

Paulette A. Torres, NRC Project Manager

11. ABSTRACT (200 words or less)

This report describes studies conducted at Argonne National Laboratory on the potential for chemical effects on head loss across sump screens. Three different buffering solutions were used for these tests: trisodium phosphate, sodium hydroxide, and sodium tetraborate. These pH control agents used following a LOCA at at a nuclear power plant show various degrees of interaction with the insulating materials Cal-Sil and NUKON. Results for Cal–Sil dissolution tests in TSP solutions, settling rate tests of calcium phosphate precipitates, and benchmark tests in chemically inactive environments are also presented. The objective of the head loss tests was to assess the head loss produced by debris beds created by Cal–Sil, fibrous debris, and calcium phosphate precipitates. The effects of both the relative arrival time of the precipitates and insulation debris and the calcium phosphate formation process were specifically evaluated. The debris loadings, test loop flow rates, and test temperature were chosen to be reasonably representative of those expected in plants with updated sump screen configurations, although the approach velocity of 0.1 ft/s used for most of the tests is 3–10 times that expected in plants with large screens . Other variables were selected with the intent to reasonably bound the head loss variability due to arrival time and calcium phosphate formation uncertainty. Settling tests were conducted to measure the settling rates of calcium phosphate precipitates (formed by adding dissolved Ca to boric acid and TSP solutions) in water columns having no bulk directional flow.

Dissolved Al concentrations of 100 ppm were shown to lead to large pressure drops for the screen area to sump volume ratio and fiber debris bed studied. No chemical effects on head loss were observed in sodium tetraborate buffered solutions even for environments with high ratios of submerged Al area to sump volume

12. KEY WORDS/DESCRIPTORS *(List words or phrases that will assist researchers in locating this report.)*

Generic Safety Issue 191
Chemical Effects
Head-Loss
Sump strainer
Loss of coolant accident (LOCA)

13. AVAILABILITY STATEMENT
unlimited

14. SECURITY CLASSIFICATION
(This Page)
unclassified
(This Report)
unclassified

15. NUMBER OF PAGES

16.PRICE

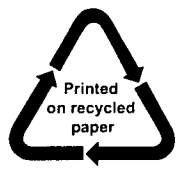

Federal Recycling Program

UNITED STATES
NUCLEAR REGULATORY COMMISSION
WASHINGTON, DC 20555-0001

OFFICIAL BUSINESS